RESEARCH ARTICLE OPEN ACCESS

Exosome Tethering Requires Tetherin Homodimerisation

Yağmur Yıldızhan[1] | Adam M. Bourke[1] | Hannah K. Jackson[1,2] | Paul T. Manna[3] | Roberta Palmulli[1,4] | James R. Edgar[1]

[1]Department of Pathology, University of Cambridge, Cambridge, UK | [2]Children's Brain Tumour Research Centre, Biodiscovery Institute, University of Nottingham, Nottingham, UK | [3]Holtra AB, Gothenburg, Sweden | [4]Department of Biochemistry, University of Cambridge, Cambridge, UK

Correspondence: James R. Edgar (je333@cam.ac.uk)

Received: 7 August 2025 | **Revised:** 25 November 2025 | **Accepted:** 4 December 2025

Keywords: exosomes | extracellular vesicles | membrane trafficking | tethering

ABSTRACT

Exosomes are small extracellular vesicles that originate as intraluminal vesicles (ILVs) within multivesicular bodies (MVBs). Upon fusion of MVBs with the plasma membrane, ILVs are released into the extracellular environment as exosomes. Although exosomes can diffuse away from their cells of origin, the expression of the antiviral restriction factor tetherin promotes their retention at the cell surface, thereby limiting their release into the extracellular milieu. Tetherin plays an analogous role in retaining other extracellular particles, including many enveloped viruses and midbody remnants. We hypothesised that tetherin physically links exosomes to the cell surface through specific structural features of the protein. To test this, we combined biochemical assays with live-cell and ultrastructural imaging approaches to determine which elements of tetherin are required for exosome retention. Our analysis shows that the formation of tetherin homodimers is essential for exosome tethering. Mutations in regions or motifs of tetherin predicted to impact tetherin traffic to ILVs have only minor impacts on exosome tethering, suggesting redundancy in the mechanisms of tetherin traffic to ILVs, and subsequently, to exosomes. Collectively, these findings provide the first molecular insights into the mechanism that govern exosome tethering.

1 | Introduction

Multivesicular bodies (MVBs) are specialised endosomal compartments that play a vital role in the sorting and trafficking of proteins, lipids and other cellular components. A hallmark of MVBs is the presence of intraluminal vesicles (ILVs), which form through the inward budding of the MVB limiting membrane (Hirsch et al. 1968). This process encloses specific cargo, including proteins, RNA and lipids, into ILVs, which are destined either for degradation within lysosomes (Felder et al. 1990) or for release into the extracellular environment (Harding et al. 1983; Pan and Johnstone 1983; Raposo et al. 1996). ILVs can be generated through both ESCRT-dependent (Hurley and Hanson 2010; Raiborg and Stenmark 2009) and ESCRT-independent pathways (Edgar et al. 2014; Stuffers et al. 2009; Theos et al. 2006; van Niel et al. 2011), and different subtypes of ILVs coexist within single MVBs (Edgar et al. 2014). Once MVBs are formed, they follow one of two primary routes: fusion with the lysosome for degradation of ILVs, or fusion with the plasma membrane leading to the release of ILVs into the extracellular space, where they are designated as exosomes (Raposo et al. 1996).

Exosomes play a crucial role in intercellular communication by transferring bioactive molecules between cells, influencing physiological and pathological processes such as immune modulation (Bobrie et al. 2011; Muntasell et al. 2007; Nolte-'t Hoen et al. 2009; Théry et al. 2002), skin pigmentation (Lo Cicero et al. 2015; Prospéri et al. 2024), tumour progression (Hoshino et al. 2013; Palmulli et al. 2025; Peinado et al. 2012) and the propagation of pathogenic proteins including Prions (Fevrier et al. 2004), beta amyloid (Rajendran et al. 2006) and alpha synuclein (Emmanouilidou et al. 2010).

This is an open access article under the terms of the Creative Commons Attribution License, which permits use, distribution and reproduction in any medium, provided the original work is properly cited.

© 2025 The Author(s). *Biology of the Cell* published by Wiley-VCH GmbH on behalf of Société Française des Microscopies and Société de Biologie Cellulaire de France.

Historically, exosomes were believed to be released from cells to diffuse freely into the extracellular space to act on cells in *trans*. Our previous work, however, demonstrated instead that exosomes can also be retained at the plasma membrane of the producer cell through a process mediated by the antiviral restriction factor tetherin (*Bst2*/CD317) (Edgar et al. 2016). The observation that exosomes remain tethered to the plasma membrane highlighted additional possible functions for exosomes, and largely that tethered exosomes could provide a high local concentration of molecules at the cell surface that are not subject to lateral diffusion in the same way as those at the plasma membrane. Tetherin is widely expressed, and its expression is highly sensitive to interferon (Neil et al. 2007). Although numerous published micrographs show clusters of exosomes at the surface of cells, the function of tethered exosomes remains largely unknown. Tethered exosomes have recently been found to contribute to the degradation of the pericellular extracellular matrix in breast cancers (Palmulli et al. 2025), and this finding may explain the previously unresolved link between tetherin overexpression in metastatic cancers and metastasis formation (Mahauad-Fernandez and Okeoma 2017; Mahauad-Fernandez et al. 2014).

In addition to exosomes, tetherin mediates the retention of other extracellular particles, including enveloped viruses (Kaletsky et al. 2009; Lopez et al. 2010; Mansouri et al. 2009; Neil et al. 2008; Stewart et al. 2023; Wang et al. 2014) and midbody remnants (Presle et al. 2021), highlighting its broad role in regulating the retention and release of small membranous particles that are generated by outward budding. The formation of exosomes, enveloped viruses and midbody remnants occurs via membrane budding events directed away from the cytosol—either towards the extracellular space or into the lumen of endosomes. These outward budding processes utilise specialised molecular machinery. Cytokinesis, which results in the formation of midbody remnants, as well as the biogenesis of a subset of ILV/exosomes and enveloped viruses, involves the Endosomal Sorting Complex Required for Transport (ESCRT) machinery (McDonald and Martin-Serrano 2009). Whether tetherin also restricts other forms of extracellular vesicles, such as ectosomes and apoptotic bodies, remains unclear.

Human tetherin consists of a short N-terminal cytosolic domain, a transmembrane domain and an extracellular coiled-coil domain, which is anchored to the membrane via a C-terminal GPI anchor (Kupzig et al. 2003). The extracellular coiled-coil domain contains three conserved cysteine residues essential for homodimer formation, a key requirement for the retention of both human immunodeficiency virus-1 (HIV-1) particles (Perez-Caballero et al. 2009) and midbody remnants (Presle et al. 2021). Although the structural features of tetherin are well characterised in the context of viral restriction, their role in exosome tethering remains poorly understood. Determining which structural elements are required for exosome retention is crucial for elucidating the molecular mechanisms that regulate exosome release and surface accumulation.

In this study, we aim to elucidate the molecular mechanism underlying tetherin-mediated exosome tethering. Using a combination of molecular, biochemical, live-cell and ultrastructural imaging approaches, we demonstrated that tetherin homodimer formation is crucial for exosome tethering. By generating tetherin mutants that disrupt specific functions, such as dimerisation, ubiquitination and the addition of a GPI anchor, we assessed their impact on exosome retention. We also examined the molecular machinery that traffics tetherin to ILVs, and which features of tetherin mediate this trafficking. Together, our results provided the first mechanistic insights into how tetherin controls exosome retention at the plasma membrane and clarified the structural determinants underlying this function.

2 | Materials and Methods

2.1 | Cell Lines and Standard Culture Conditions

WT HeLa cells were a gift from Professor Scottie Robinson (CIMR, University of Cambridge, UK). Bst2KO HeLa cells were previously described (Edgar et al. 2016). HEK293T cells were purchased from ATCC. MelJuSo cells were a gift from Dr Claire Shannon-Lowe (University of Birmingham). All cell lines were cultured in DMEM supplemented with 10% foetal bovine serum and 1% penicillin/streptomycin, and maintained at 37°C in a 5% CO_2 incubator.

Bst2KO MelJuSo cells were generated using px330-Bst2 and the gRNA (5′-GCTCCTGATCATCGTGATTC**TGG)** as previously described (Edgar et al. 2016). Bst2KO MelJuSo cells were bulk sorted by FACS, expanded and verified by Western blot, flow cytometry and immunofluorescence (as shown in Figure 5).

All cells were regularly screened for mycoplasma using a PCR Mycoplasma detection kit (Abcam, ab289834).

2.2 | Cloning

cDNAs for Bst2-WT-HA, Bst2-C3A-HA, Bst2-K18A-HA, Bst2-Nterm-HA and Bst2-GPI-HA were a gift from Professor George Banting (University of Bristol, UK) and are previously described (Billcliff et al. 2013). HA-tagged tetherin cDNAs were PCR'ed to add NotI and XhoI restriction sites and cloned into the retroviral vector, pQCXIH.

cDNAs for Bst2-WT-mScar and Bst2-C3A-mScar were synthesised by GeneWiz (Azenta Life Sciences) and cloned to pQCXIH between AgeI and BamHI restriction sites. mScarlet cDNA was cloned between position Y154/P155 of human *Bst2* and separated by short, flexible (Gly/Ser) linkers.

pCMV-Sport6-CD63-pHluorin was a gift from Dr Michiel Pegtel (Amsterdam UMC, Netherlands).

All plasmids were confirmed by Sanger sequencing. Sequences are provided in Table 1.

2.3 | Generation of Tetherin Rescue Cell Lines

Retroviral pQCXIH vectors were cotransfected into HEK293T cells with pMD.GagPol and pMD.VSVG packaging plasmids using TransIT-293 (Mirus Bio, USA). Viral supernatants were

TABLE 1 | Nucleotide sequences for constructs used in this study.

Construct	Amino acid sequence	Nucleotide sequence
Bst2-HA	ATGGCATCTACTTCGTATGACTATTGCAGAGTGCCCATG- GAAGACGGGGATAAGCGCTGTAAGCTTCTGCTGGGG- ATAGGAATTCTGGTGCTCCTGATCATCGTGATTCTG- GGGGTGCCCTTGATTATCTTCACCATCAAGGCCAA- CAGCGAGGCCTGCCGGGACGGCCTTCGGGCAGT- GATGGAGTGTCGCAATGTCACCCATCTCCTGCAA- CAAGAGCTGACCGAGGCCCAGAAGGGCTTTCAGGA- TGTGGAGGCCCAGGCCGCCACCTGCAACCACACT- GTGATGGCCCTAATGGCTTCCCTGGATGCAGAG- AAGGCCCAAGGACAAAAGAAAGTGGAGGAG- CTTGAGGGAGAGATCACTACATTAAACCATAAGC- TTCAGGACGCGTCTGCAGAGGTGGAGCGACTGAGA- AGAGAAAACCAGGTCTTAAGCGTGAGAATCGCG- GACAAGAAGTACTACGGCCGGCCATACCCATAC- CCATACGACGTCCCAGACTACGCTGCTAGCCCCAG- CTCCCAGGACTCCAGCTCCGCTGCGGCGCCCCAGC- TGCTGATTGTGCTGCTGGGCCTCAGCGCTCTGCTGCAGTGA	MASTSYDYCRVPMEDGDKRCK LLLGIGILVLLIIVILGVPLI IFTIKANSEACRDGLRAVMEC RNVTHLLQQELTEAQKGFQDV EAQAATCNHTVMALMASLDAE KAQGQKKVEELEGEITTLNHK LQDASAEVERLRRENQVLSVR IADKKYYGRPYPYPYDVPDYAASPSS QDSSSAAAPQLLIVLLGLSALLQ*
C3A-HA	ATGGCATCTACTTCGTATGACTATTGCAGAGTGCC CATGGAAGACGGGGATAAGCGCTGTAAGCTTCTGCTGGG GATAGGAATTCTGGTGCTCCTGATCATCGTGATTCTGGG GGTGCCCTTGATTATCTTCACCATCAAGGCCAACAGCGA GGCCGCCCGGGACGGCCTTCGGGCAGTGATGGAGGCTCG CAATGTCACCCATCTCCTGCAACAAGAGCTGACCGAGGC CCAGAAGGGCTTTCAGGATGTGGAGGCCCAGGCCGCCAC CGCCAACCACACTGTGATGGCCCTAATGGCTTCCCTGGA TGCAGAGAAGGCCCAAGGACAAAAGAAAGTGGAGGAGCT TGAGGGAGAGATCACTACATTAAACCATAAGCTTCAGGA CGCGTCTGCAGAGGTGGAGCGACTGAGAAGAGAAAACCA GGTCTTAAGCGTGAGAATTGCCGATAAGAAGTACTACGG CCGGCCATACCCATACCCATACGACGTCCCAGACTACGC TGCTAGCCCCAGCTCCCAGGACTCCAGCTCCGCTGCGGC GCCCCAGCTGCTGATTGTGCTGCTGGGCCTCAGCGCTCT- GCTGCAGTGA	MASTSYDYCRVPMEDGDKRCK LLLGIGILVLLIIVILGVPLI IFTIKANSEAARDGLRAVMEA RNVTHLLQQELTEAQKGFQDV EAQAATANHTVMALMASLDAE KAQGQKKVEELEGEITTLNHK LQDASAEVERLRRENQVLSVR IADKKYYGRPYPYPYDVPDYAAS- PSSQDSSSAAAPQLLIVLLGLSALLQ*
K18A-HA	ATGGCATCTACTTCGTATGACTATTGCAGAGTGCCC- ATGGAAGACGGGGATgcaCGCTGTAAGCTTCTGCTG- GGGATAGGAATTCTGGTGCTCCTGATCATCGTGATT- CTGGGGGTGCCCTTGATTATCTTCACCATCAAGGCC- AACAGCGAGGCCTGCCGGGACGGCCTTCGGGCAGT- GATGGAGTGTCGCAATGTCACCCATCTCCTGCAACA- AGAGCTGACCGAGGCCCAGAAGGGCTTTCAGGATG- TGGAGGCCCAGGCCGCCACCTGCAACCACACTGTG- ATGGCCCTAATGGCTTCCCTGGATGCAGAGAAGGCC- CAAGGACAAAAGAAAGTGGAGGAGCTTGAGGGAGA- GATCACTACATTAAACCATAAGCTTCAGGACGCGTCT- GCAGAGGTGGAGCGACTGAGAAGAGAAAACCAGGTC- TTAAGCGTGAGAATCGCGGACAAGAAGTACTACGGCC- GGCCATACCCATACCCATACGACGTCCCAGACTACGCT- GCTAGCCCCAGCTCCCAGGACTCCAGCTCCGCTGCGG- CGCCCCAGCTGCTGATTGTGCTGCTGGG- CCTCAGCGCTCTGCTGCAGTGA	MASTSYDYCRVPMEDGDARCK LLLGIGILVLLIIVILGVPLI IFTIKANSEACRDGLRAVMEC RNVTHLLQQELTEAQKGFQDV EAQAATCNHTVMALMASLDAE KAQGQKKVEELEGEITTLNHK LQDASAEVERLRRENQVLSVR IADKKYYGRPYPYPYDVPDYAASPS- SQDSSSAAAPQLLIVLLGLSALLQ*
Nterm-HA	ATGAAGCTTCTGCTGGGGATAGGAATTCTGGTGCTCCTGA- TCATCGTGATTCTGGGGGTGCCCTTGATTATCTTCACC- ATCAAGGCCAACAGCGAGGCCTGCCGGGACGGCCTT- CGGGCAGTGATGGAGTGTCGCAATGTCACCCATCTCC	MKLLLGIGILVLLIIVILGVP LIIFTIKANSEACRDGLRAVM ECRNVTHLLQQELTEAQKGFQ DVEAQAATCNHTVMALMASLD

(Continues)

TABLE 1 | (Continued)

Construct	Amino acid sequence	Nucleotide sequence
		AEKAQGQKKVEELEGEITTLN HKLQDASAEVERLRRENQVLS VRIADKKYYGRPYPYPYDVPDYAAS- PSSQDSSSAAAPQLLIVLLGLSALLQ*
GPI-HA	ATGGCATCTACTTCGTATGACTATTGCAGAGTGCCCATGGA- AGACGGGGATAAGCGCTGTAAGCTTCTGCTGGGGATAGGA- ATTCTGGTGCTCCTGATCATCGTGATTCTGGGGGTGCCCTT- GATTATCTTCACCATCAAGGCCAACAGCGAGGCCTGCCGG- GACGGCCTTCGGGCAGTGATGGAGTGTCGCAATGTCACCC- ATCTCCTGCAACAAGAGCTGACCGAGGCCCAGAAGGGCTT- TCAGGATGTGGAGGCCCAGGCCGCCACCTGCAACCACACT- GTGATGGCCCTAATGGCTTCCCTGGATGCAGAGAAGGCCC- AAGGACAAAAGAAAGTGGAGGAGCTTGAGGGAGAGATCA- CTACATTAAACCATAAGCTTCAGGACGCGTCTGCAGAGGTG- GAGCGACTGAGAAGAGAAAACCAGGTCTTAAGCGTGAGAA- TCGCGGACAAGAAGTACTACGGCCGGCCATACCCATACCCA- TACGACGTCCCAGACTACGCTGCTAGCC- CCAGCTCCCAGGACTCCTAG	MASTSYDYCRVPMEDGDKRCK LLLGIGILVLLIIVILGVPLI IFTIKANSEACRDGLRAVMEC RNVTHLLQQELTEAQKGFQDV EAQAATCNHTVMALMASLDAE KAQGQKKVEELEGEITTLNHK LQDASAEVERLRRENQVLSVRIA- DKKYYGRPYPYPYDVPDYAASPSSQDS*
Bst2-mScar	ATGGCATCTACTTCGTATGACTATTGCAGAGTGCCCATGGA- AGACGGGGATAAGCGCTGTAAGCTTCTGCTGGGGATAGGA- ATTCTGGTGCTCCTGATCATCGTGATTCTGGGGGTGCCCT- TGATTATCTTCACCATCAAGGCCAACAGCGAGGCCTGCCGG- GACGGCCTTCGGGCAGTGATGGAGTGTCGCAATGTCACCC- ATCTCCTGCAACAAGAGCTGACCGAGGCCCAGAAGGGCTT- TCAGGATGTGGAGGCCCAGGCCGCCACCTGCAACCACACT- GTGATGGCCCTAATGGCTTCCCTGGATGCAGAGAAGGCCC- AAGGACAAAAGAAAGTGGAGGAGCTTGAGGGAGAGATCA- CTACATTAAACCATAAGCTTCAGGACGCGTCTGCAGAGGTG- GAGCGACTGAGAAGAGAAAACCAGGTCTTAAGCGTGAGAA- TCGCGGACAAGAAGTACTACggaggcagcggtATGGTGAGCAAG- GGCGAGGCAGTGATCAAGGAGTTCATGCGGTTCAAGGTGC- ACATGGAGGGCTCCATGAACGGCCACGAGTTCGAGATCG- AGGGCGAGGGCGAGGGCCGCCCCTACGAGGGCACCCAGA- CCGCCAAGCTGAAGGTGACCAAGGGTGGCCCCCTGCCCTT- CTCCTGGGACATCCTGTCCCCTCAGTTCATGTACGGCTCCA- GGGCCTTCACCAAGCACCCCGCCGACATCCCCGACTACTA- TAAGCAGTCCTTCCCCGAGGGCTTCAAGTGGGAGCGCGTG- ATGAACTTCGAGGACGGCGGCGCCGTGACCGTGACCCAG- GACACCTCCCTGGAGGACGGCACCCTGATCTACAAGGTGA- AGCTCCGCGGCACCAACTTCCCTCCTGACGGCCCCGTAAT- GCAGAAGAAGACAATGGGCTGGGAAGCGTCCACCGAGCG- GTTGTACCCCGAGGACGGCGTGCTGAAGGGCGACATTAAG- ATGGCCCTGCGCCTGAAGGACGGCGGCCGCTACCTGGCGG- ACTTCAAGACCACCTACAAGGCCAAGAAGCCCGTGCAGAT- GCCCGGCGCCTACAACGTCGACCGCAAGTTGGACATCACC- TCCCACAACGAGGACTACACCGTGGTGGAACAGTACGAAC- GCTCCGAGGGCCGCCACTCCACCGGCGGCATGGACGAGC- TGTACAAGggaggcCCCAGCTCCCAGGACTCCAGCTCCGCT- GCGGCGCCCCAGCTGCTGATTGTGCTGCTGGGC- CTCAGCGCTCTGCTGCAGTGA	MASTSYDYCRVPMEDGDKRCK LLLGIGILVLLIIVILGVPLI IFTIKANSEACRDGLRAVMEC RNVTHLLQQELTEAQKGFQDV EAQAATCNHTVMALMASLDAE KAQGQKKVEELEGEITTLNHK LQDASAEVERLRRENQVLSVR IADKKYYGGSGMVSKGEAVIKEF- MRFKVHMEGSMNGHEFEIEGEG- EGRPYEGTQTAKLKVTKGGPL- PFSWDILSPQFMYGSRAFTKH- PADIPDYYKQSFPEGFKWERV- MNFEDGGAVTVTQDTSLEDGTL- IYKVKLRGTNFPPDGPVMQK- KTMGWEASTERLYPEDGVLKGD- IKMALRLKDGGRYLADFKTTY- KAKKPVQMPGAYNVDRKLDI- TSHNEDYTVVEQYERSEGRHS- TGGMDELYKGGPSSQDSSSA- AAPQLLIVLLGLSALLQ*

(Continues)

TABLE 1 | (Continued)

Construct	Amino acid sequence	Nucleotide sequence
C3A-mScar	ATGGCATCTACTTCGTATGACTATTGCAGAGTG CCCATGGAAGACGGGGATAAGCGCGCAAAGCTT CTGCTGGGGATAGGAATTCTGGTGCTCCTGATC ATCGTGATTCTGGGGGTGCCCTTGATTATCTTC ACCATCAAGGCCAACAGCGAGGCCGCACGGGAC GGCCTTCGGGCAGTGATGGAGGCACGCAATGTC ACCCATCTCCTGCAACAAGAGCTGACCGAGGCC CAGAAGGGCTTTCAGGATGTGGAGGCCCAGGCC GCCACCGCAAACCACACTGTGATGGCCCTAATG GCTTCCCTGGATGCAGAGAAGGCCCAAGGACAA AAGAAAGTGGAGGAGCTTGAGGGAGAGATCACT ACATTAAACCATAAGCTTCAGGACGCGTCTGCA GAGGTGGAGCGACTGAGAAGAGAAAACCAGGTC TTAAGCGTGAGAATCGCGGACAAGAAGTACTAC ggaggcagcggtATGGTGAGCAAGGGCGAGGCA GTGATCAAGGAGTTCATGCGGTTCAAGGTGCAC ATGGAGGGCTCCATGAACGGCCACGAGTTCGAG ATCGAGGGCGAGGGCGAGGGCCGCCCCTACGAG GGCACCCAGACCGCCAAGCTGAAGGTGACCAAG GGTGGCCCCCTGCCCTTCTCCTGGGACATCCTG TCCCCTCAGTTCATGTACGGCTCCAGGGCCTTC ACCAAGCACCCCGCCGACATCCCCGACTACTAT AAGCAGTCCTTCCCCGAGGGCTTCAAGTGGGAG CGCGTGATGAACTTCGAGGACGGCGGCGCCGTG ACCGTGACCCAGGACACCTCCCTGGAGGACGGC ACCCTGATCTACAAGGTGAAGCTCCGCGGCACC AACTTCCCTCCTGACGGCCCCGTAATGCAGAAG AAGACAATGGGCTGGGAAGCGTCCACCGAGCGG TTGTACCCCGAGGACGGCGTGCTGAAGGGCGAC ATTAAGATGGCCCTGCGCCTGAAGGACGGCGGC CGCTACCTGGCGGACTTCAAGACCACCTACAAG GCCAAGAAGCCCGTGCAGATGCCCGGCGCCTAC AACGTCGACCGCAAGTTGGACATCACCTCCCAC AACGAGGACTACACCGTGGTGGAACAGTACGAA CGCTCCGAGGGCCGCCACTCCACCGGCGGCATG GACGAGCTGTACAAGggaggcCCCAGCTCCCAG GACTCCAGCTCCGCTGCGGCGCCCCAGCTGCTG ATTGTGCTGCTGGGCCTCAGCGCTCTGCTGCAGTGA	MASTSYDYCRVPMEDGDKRAK LLLGIGILVLLIIVILGVPLI IFTIKANSEAARDGLRAVMEA RNVTHLLQQELTEAQKGFQDV EAQAATANHTVMALMASLDAE KAQGQKKVEELEGEITTLNHK LQDASAEVERLRRENQVLSVR IADKKYYGGSGMVSKGEAVIKEFM- RFKVHMEGSMNGHEFEIEGEGE- GRPYEGTQTAKLKVTKGGPLP- FSWDILSPQFMYGSRAFTKHP- ADIPDYYKQSFPEGFKWERVM- NFEDGGAVTVTQDTSLEDGT- LIYKVKLRGTNFPPDGPVMQKK- TMGWEASTERLYPEDGVLKG- DIKMALRLKDGGRYLADFKTT- YKAKKPVQMPGAYNVDRKLDI- TSHNEDYTVVEQYERSEGRH- STGGMDELYKGGPSSQDSSSAAAP- QLLIVLLGLSALLQ*
Forced Dimer-HA (FD-HA)	ATGGCATCTACTTCGTATGACTATTGCAGAGTGC CCATGGAAGACGGGGATAAGCGCTGTAAGCTTCT GCTGGGGATAGGAATTCTGGTGCTCCTGATCATC GTGATTCTGGGGGTGCCCTTGATTATCTTCACCA TCAAGGCCAACAGCGAGGCCGCCCGGGACGGCCT TCGGGCAGTGATGGAGGCTCGCAATGTCACCCAT CTCCTGCAACAAGAGCTGACCGAGGCCTGCAAGG GCTTTCAGGATTGTGAGGCCCAGGCCGCCACCGC CAACCACACTGTGATGGCCCTAATGGCTTCCCTG GATGCAGAGAAGGCCCAAGGACAAAAGAAAGTGG AGGAGCTTGAGGGAGAGATCACTACATTAAACCA TAAGCTTCAGGACGCGTCTGCAGAGGTGGAGCGA CTGAGAAGAGAATGCCAGGTCTTAAGCGTGAGAA TTGCCGATAAGAAGTACTACGGCCGGCCATACCC ATACCCATACGACGTCCCAGACTACGCTGCTAGC CCCAGCTCCCAGGACTCCAGCTCCGCTGCGGCGC CCCAGCTGCTGATTGTGCTGCTGGGCCTCAGCGC TCTGCTGCAGTGA	MASTSYDYCRVPMEDGDKRCK LLLGIGILVLLIIVILGVPLI IFTIKANSEAARDGLRAVMEA RNVTHLLQQELTEACKGFQDC EAQAATANHTVMALMASLDAE KAQGQKKVEELEGEITTLNHK LQDASAEVERLRRECQVLSVR IADKKYYGRPYPYPYDVPDYA ASPSSQDSSSAAAPQLLIVLL GLSALLQ*

collected 48 h after transfection, passed through 0.45 μm filters to remove dead cells and debris. Recipient cells were transduced by 'spinfection'—viral supernatants were centrifuged at 1800 rpm in a benchtop centrifuge at 37°C for 70 min to enhance viral transduction. Four days posttransduction, cells were subject to antibiotic selection with 200 μg/mL Hygromycin B.

HA- and mScar-tetherin stable cell lines were generated by retroviral transduction of Bst2KO HeLa or Bst2KO MelJuSo cells.

2.4 | Antibodies

The following primary antibodies were used: anti-tetherin (rabbit monoclonal, Abcam, ab243230, WB 1:2500, IF 1:200, immunoEM 1:20), anti-EEA1 (mouse monoclonal, BD Transduction, 610457, IF 1:200), anti-VPS35 (mouse monoclonal, Santa Cruz, B-5, IF 1:200), anti-CD63 (mouse monoclonal, BioLegend, H5C6, WB 1:1000, IF 1:200), anti-LAMP1 (mouse monoclonal, BioLegend, H4A3, IF 1:200), anti-CIMPR (mouse monoclonal, Abcam, ab2733, IF 1:200), anti-GM130 (mouse monoclonal, BD Biosystems, 35/GM130, IF 1:200, WB 1:1000), anti-GAPDH (mouse monoclonal, Proteintech, 1E6D9, WB 1:10,000), anti-LBPA (mouse monoclonal, Millipore, 6C4, IF 1:200), anti-HA (rat monoclonal, Roche, 3F10, IF 1:200), anti-HA (rabbit monoclonal, Cell Signalling, C29F4, WB 1:1000, immunoEM 1:30), anti-ALIX (mouse monoclonal, GeneTex, 3A9, WB 1:1000), anti-Syntenin (rabbit monoclonal, Abcam, ab133267, WB 1:1000), anti-Tsg101 (mouse monoclonal, GeneTex, 4A10, WB 1:1000), anti-CD9 (rabbit monoclonal, Abcam, ab92726, WB 1:500), anti-Hrs (rabbit polyclonal, a gift from Prof Sylvié) and anti-HLA-DR (rabbit monoclonal, abcam, ab259258, WB 1:1000). PE-conjugated anti-Bst2 (mouse monocloncal, BioLegend, RS38E, FC 1:200), APC-conjugated anti-HA (Mouse monocloncal, Miltenyi, CG8-1F3.3.1, FC 1:200).

Secondary antibodies used in the study were: anti-rat IgG Alexa-488 (goat, Molecular Probe, A11006, IF 1:200), anti-rabbit IgG Alexa 488/555 (goat, ThermoFisher, IF 1:200) and anti-mouse IgG Alexa-488/555 (goat, ThermoFisher, IF 1:200). For Western blotting, anti-mouse IRDye 800CW (goat, LI-COR, 926-32210, WB 1:10,000) and anti-rabbit IRDye 680RD (goat, LI-COR, 926-68071, WB 1:10,000) were used.

2.5 | Reagents and Small Molecules

Leupeptin hemisulphate was purchased from Cambridge Bioscience (HY-18234A-1 mL), recombinant human IFN-gamma from PeproTech (300-02-100UG), Lipofectamine 2000 from Invitrogen (11668-030) and Bafilomycin A1 was from Sigma–Aldrich (B1793).

2.6 | Western Blotting

Whole cells or exosome-enriched pellets were lysed in lysis buffer (1% Triton-X100, 1 mM EDTA, 150 mM NaCl, 20 mM Tris pH 7.5) supplemented with 1x cOmplete EDTA-free Protease Inhibitor Cocktail (11836170001, Roche) on ice for 30 min with regular vortexing. Lysates were centrifuged at 14,000 × *g* for 15 min at 4°C. Resultant lysates were mixed with 4x NuPage LDS sample buffer (ThermoFisher), boiled at 65 or 95°C for 10 min and subjected to SDS-PAGE on NuPage 4%–12% Bis-Tris precast gels (ThermoFisher). Samples were transferred to PVDF membranes. Membranes were blocked in 5% nonfat dried milk in PBS with 0.1% Tween-20 (PBS-T) for 30 min at room temperature. Then, they were incubated with primary antibodies overnight at 4°C, followed by secondary antibodies for 1 h at room temperature. Finally, the membranes were imaged with an Odyssey CLx system (LI-COR).

Signal intensities were quantified using ImageJ Fiji software, with quantifications based on at least three independent experiments. The presented immunoblots are representative of these experiments.

2.7 | Immunofluorescence Microscopy

Cells were seeded to 13 mm glass coverslips and left overnight to adhere. The following day, cells were fixed with 4% PFA/PBS. Cells were quenched with 15 mM glycine/PBS and permeabilised using 0.1% saponin/PBS. Blocking and subsequent antibody labelling were performed with 1% BSA supplemented with 0.01% saponin/PBS. Nuclei were labelled with Hoechst. Cells were mounted to slides with mounting medium, and images were acquired using a LSM700 confocal microscope (63×, 1.4nA, oil immersion objectives; ZEISS).

2.8 | Colocalisation Analysis

ImageJ Fiji version 2.3.0 was used for colocalisation analysis. Pearsons' and Mander's correlation coefficient between two channels was quantified using JACoP plugin of ImageJ Fiji software. At least 20 cells from three independent experiments were analysed for each condition.

2.9 | Immunofluorescence Analysis—CD63 Particle Density

Immunofluorescence images were analysed using ImageJ Fiji version 2.3.0 to quantify CD63-positive particle count over cell area. Images were converted to 8-bit and background-subtracted. A consistent threshold was applied across all samples to segment CD63-positive puncta. The 'Analyse Particles' function was used to count individual puncta. For each image, the cell area was manually outlined, and CD63 particle counts were normalised to the cell area. Particle density was calculated as: (number of CD63-positive particles/cell area in μm^2) × 100. This yielded density values expressed as particles per 100 μm. Data were analysed using GraphPad Prism. Group comparisons were performed using ordinary one-way ANOVA followed by Tukey's multiple comparisons test. $p > 0.05$ (ns), $p \leq 0.05$ (*), $p \leq 0.01$ (**), $p \leq 0.001$ (***) and $p \leq 0.0001$ (****).

2.10 | Flow Cytometry

Cells were gently trypsinised and centrifuged at 350 × *g* for 4 min at 4°C. Cell pellets were resuspended in FACS buffer

(PBS containing 1% BSA and 1 mM EDTA), transferred to 96-well plates and washed once. For intracellular staining, cells were fixed, permeabilised with 0.1% saponin in FACS buffer, then incubated with fluorophore-conjugated antibodies diluted in 0.05% saponin/FACS buffer for 45 min on ice. For surface staining, cells were incubated with fluorophore-conjugated antibodies in FACS buffer for 45 min on ice. For staining with unconjugated primary antibodies, cells were incubated with the primary antibody for 45 min, washed and subsequently incubated with Alexa-conjugated secondary antibodies. Before data acquisition, cells were washed twice with cold PBS. Fluorescence intensity was analysed using a Cytoflex LX flow cytometer (Beckman Coulter) equipped with six lasers (488, 561 and 638 nm lasers were used).

2.11 | siRNA-Mediated Knockdown of Hrs

Cells were transfected with ON-TARGETplus siHrs pool (*Hgs*) (Horizon Discovery) using Lipofectamine RNAiMax (ThermoFisher) on Days 1 and 2 and harvested on Day 4. Non-targeting siRNA was used as a control (ON-TARGETplus Non-targeting Pool, Horizon Discovery).

2.12 | Exosome-Enriched Preparations

Exosome-enriched preparations were generated from cell culture supernatants by differential ultracentrifugation following the protocol described in (Théry et al. 2006). Briefly, cells were cultured in equal numbers on three T175 tissue culture flasks containing 30 mL of media. To induce exosome release, cells were treated with 100 nM Bafilomycin A1 for 16 h. The culture supernatants were collected and centrifuged at 300 × *g* for 10 min to remove large cell debris. The supernatants were then centrifuged at 2000 × *g* for 10 min to eliminate smaller cell debris. Subsequently, the cleared supernatants were ultracentrifuged at 10,000 × *g* for 30 min using a Type 70 Ti Rotor (Beckman Coulter) to remove larger extracellular vesicles. The resulting supernatants were collected and ultracentrifuged again at 100,000 × *g* for 70 min to pellet exosomes. These pellets were washed in PBS and repelleted by ultracentrifugation at 100,000 × *g* for an additional 70 min. The final exosome-enriched pellets were either used immediately or stored at −80°C for future experiments.

2.13 | Conventional Transmission Electron Microscopy

Cells were grown on Thermanox coverslips (Nunc) and left overnight to adhere. Cells were fixed with 4% PFA/5% glutaraldehyde/0.1 M cacodylate buffer (pH 7.4) at a 1:1 ratio with culture medium (final concentration 2% PFA/2.5% glutaraldehyde) for 30 min. Cells were washed with 0.1 M cacodylate before being post-fixed with 1% osmium tetroxide: 1.5% potassium ferrocyanide. Samples were contrast enhanced using 1% tannic acid/0.1 M cacodylate buffer. Coverslips were washed with water before being dehydrated with an ethanol series. Epoxy propane was used to infiltrate cells (CY212) Epoxy resin (Agar Scientific):propylene oxide (Agar Scientific) before being infiltrated with neat CY212 Epoxy resin. Coverslips were mounted to prebaked resin stubs and polymerised overnight at 65°C. Thermanox coverslips were removed with a heat block. Seventy-nanometer sections were cut using a Diatome diamond knife mounted to an ultramicrotome and were collected to formvar-coated grids before being stained with lead citrate. An FEI Tecnai transmission electron microscope was used to visualise samples at an operating voltage of 80 kV.

2.14 | Tethered Exosome Quantification

The entire plasma membrane of each cell was examined, and all extracellular, membrane-bound vesicles with a diameter ⟨150 nm were counted. The length of the corresponding plasma membrane was measured, and the number of exosomes per micrometre of plasma membrane was calculated. Regions where cells were located within 500 nm of a neighbouring cell were excluded to minimise potential artefacts caused by adjacent cells obstructing exosome release.

To avoid bias arising from the height of the ultrathin section, at least two sections of different relative heights were analysed for each biological replicate. Two independent biological replicates were performed. Image acquisition, blinding, quantification, and subsequent unblinding were carried out in sequence. At least five independent cells were quantified per section, resulting in a minimum of 20 cells analysed per condition.

2.15 | Cryo Immunogold Transmission Electron Microscopy

Cells were fixed with 2% PFA/0.1 M phosphate buffer overnight at 4°C. Cells were scraped in 12% gelatine and immediately pelleted by centrifugation. Cell pellets were infiltrated by PVP/Sucrose before being mounted to aluminium pins, frozen in liquid nitrogen and cut at −90°C using a Diatome Diamond knife attached to a cryo ultramicrotome.

Thawed cryosections were labelled with anti-HA or anti-tetherin antibodies, before incubation with 10 nm protein-A gold. Labelled sections were stained using uranyl acetate:methyl cellulose before imaging using an FEI Tecnai transmission electron microscope at an operating voltage of 80 kV.

2.16 | Nanoparticle Tracking Analysis (NTA) With Zetaview

Exosome-enriched samples were diluted in PBS to 1 mL and pretested to ensure optimal particle concentrations (140–200 particles/frame). Measurements were performed using the ZetaView system (Particle Metrix). Each sample was analysed in three cycles, scanning 11 positions and recording 60 frames per position (video setting: high). Acquisition settings included autofocus, camera sensitivity 92.0, shutter 70, scattering intensity 4.0, at 25°C.

Videos were analysed using ZetaView Software (v8.02.31) with analysis parameters: particle size range 5–1000 and minimum brightness 20. All samples exceeded 1000 completed tracks to ensure robust quantification.

2.17 | Nanoparticle Characterisation

For DAISY analysis (HoltraAB, Gothenburg, Sweden), samples were diluted to approximately 5×10^8 particles per mL in PBS. Exosome-enriched samples were applied to microfluidic chips (Topaz, design 180, Topaz polymer, ChipShop, Jena, Germany). From each recorded particle, averaged optical properties were extracted in both digital holographic and interferometric scattering (iSCAT) imaging modes simultaneously.

2.18 | TIRF Microscopy

Total internal reflection fluorescence (TIRF) microscopy was used to monitor exosome fusion events in MelJuSo cells stably expressing either Bst2-mScarlet or C3A-mScarlet. Cells were seeded on 35 mm MatTek glass-bottom dishes (Part No.: P35G-1.5-10-C, MatTek, USA) and transiently transfected with CD63-pHluorin 24 h before imaging. Live-cell imaging was conducted using a ZEISS Elyra 7 microscope equipped with an alpha Plan-Apochromat 63×/1.46 Oil Korr M27 TIRF objective. Imaging was performed in phenol red-free complete culture medium maintained at 37°C and 5% CO_2. Time-lapse sequences were acquired at 2 or 3 Hz for a total duration of 1 min.

Fusion events—interpreted as exosome fusion or retention at the plasma membrane—were identified manually as sudden, localised increases in fluorescence intensity. Fusion activity was quantified as the number of events per μm^2 of cell surface. The duration of each event was defined as the time elapsed from the peak fluorescence intensity until the signal returned to baseline. Twenty cells were analysed across at least three biologically independent experiments to ensure reproducibility.

3 | Results

3.1 | Tetherin Distributes Throughout the Endolysosomal Pathway

Tetherin localises to a number of organelles, enabling it to restrict various extracellular particles, including enveloped viruses, midbody remnants and exosomes. The localisation of tetherin to these distinct organelles allows its incorporation into the membrane of the subsequent extracellular particle. Tetherin restricts different classes of enveloped viruses that bud from distinct organelles—for example, retroviruses (such as HIV-1) bud predominately from the plasma membrane (Morita and Sundquist 2004; Welsch et al. 2007), and coronaviruses (such as SARS-CoV-2) bud predominately into ERGIC/Golgi organelles (Goldsmith et al. 2004; Klein et al. 2020; Salanueva et al. 1999). Tetherin distribution to both the plasma membrane and to biosynthetic organelles allows it to restrict both classes of enveloped viruses. Similarly, tetherin localisation at the plasma membrane allows it to restrict midbody remnants (Presle et al. 2021). In order for tetherin to tether exosomes, it is first trafficked to ILVs of MVBs (Edgar et al. 2016)—the precursors of exosomes. The trafficking of tetherin between these organelles is therefore key to promoting its incorporation into enveloped viruses, midbody remnants and exosomes, and vital for its ability to tether such particles.

To understand the distribution of tetherin within the endolysosomal pathway, we performed confocal microscopy. Endogenous tetherin displays colocalisation with early endosomes (EEA1), late endosomes (VPS35/CD63) and lysosomes (LAMP1) (Figure 1A). Tetherin showed the highest colocalisation with VPS35 (Figure 1B)—a component of the retromer complex which traffics cargos in a retrograde direction from endosomes towards the biosynthetic pathway (Seaman et al. 1998).

Given that cholesterol-rich MVBs are more prone to fuse with the plasma membrane than lysosomes (Möbius et al. 2003), and that tetherin contains a C-terminal GPI anchor that ensures its retention in cholesterol-rich domains (Billcliff et al. 2013; Brown and Rose 1992), we examined whether tetherin-positive endosomes were also positive for cholesterol. Many tetherin puncta colocalised with cholesterol (Figure S1A), but interestingly, tetherin localised away from the LBPA, a phospholipid specifically enriched in late endosomes and lysosomes (Figure S1B).

Upon reaching endosomes, a proportion of tetherin undergoes retrograde traffic, and this enables tetherin levels to be restored in the biosynthetic pathway and plasma membrane (Stewart et al. 2023). In addition to localising to punctate organelles, tetherin displays some perinuclear staining which strongly colocalises with CIMPR, but not with the *cis*-Golgi marker GM130 (Figure 1C,D).

Late endosomes can either fuse with terminal lysosomes to form endolysosomes (Bright et al. 1997), or with the plasma membrane to release ILVs to the extracellular environment, where they become termed exosomes (Raposo et al. 1996). To determine whether tetherin-positive endosomes are selectively fated for fusion with the plasma membrane (and therefore escape from lysosomal degradation), we examined the effect of Leupeptin, a lysosomal protease inhibitor, on tetherin trafficking and abundance. Immunofluorescence microscopy revealed that treatment with Leupeptin led to an increased abundance of tetherin in LAMP1-positive organelles (Figure 1E,F), and Western blotting confirmed elevated total tetherin (Figure 1G,H). These findings collectively indicate that tetherin traffics throughout the endolysosomal pathway and that tetherin-positive late endosomes are not fated specifically for fusion with the plasma membrane.

3.2 | Tetherin Homodimer Formation Is Required for Exosome Tethering

Although the molecular mechanisms of tetherin-mediated virus and midbody remnant restriction have been elucidated, the mechanisms governing exosome tethering remain undefined (Figure 2A). One possibility is that individual tetherin molecules span opposing membranes—branching between an exosome and the plasma membrane (*branch model*). Alternatively, individual tetherin molecules may be embedded in a single membrane but form disulfide-linked homodimers with tetherin molecules in an opposing membrane (*homodimer model*).

To define the molecular mechanisms of exosome tethering, we generated several tetherin mutants, which we stably expressed

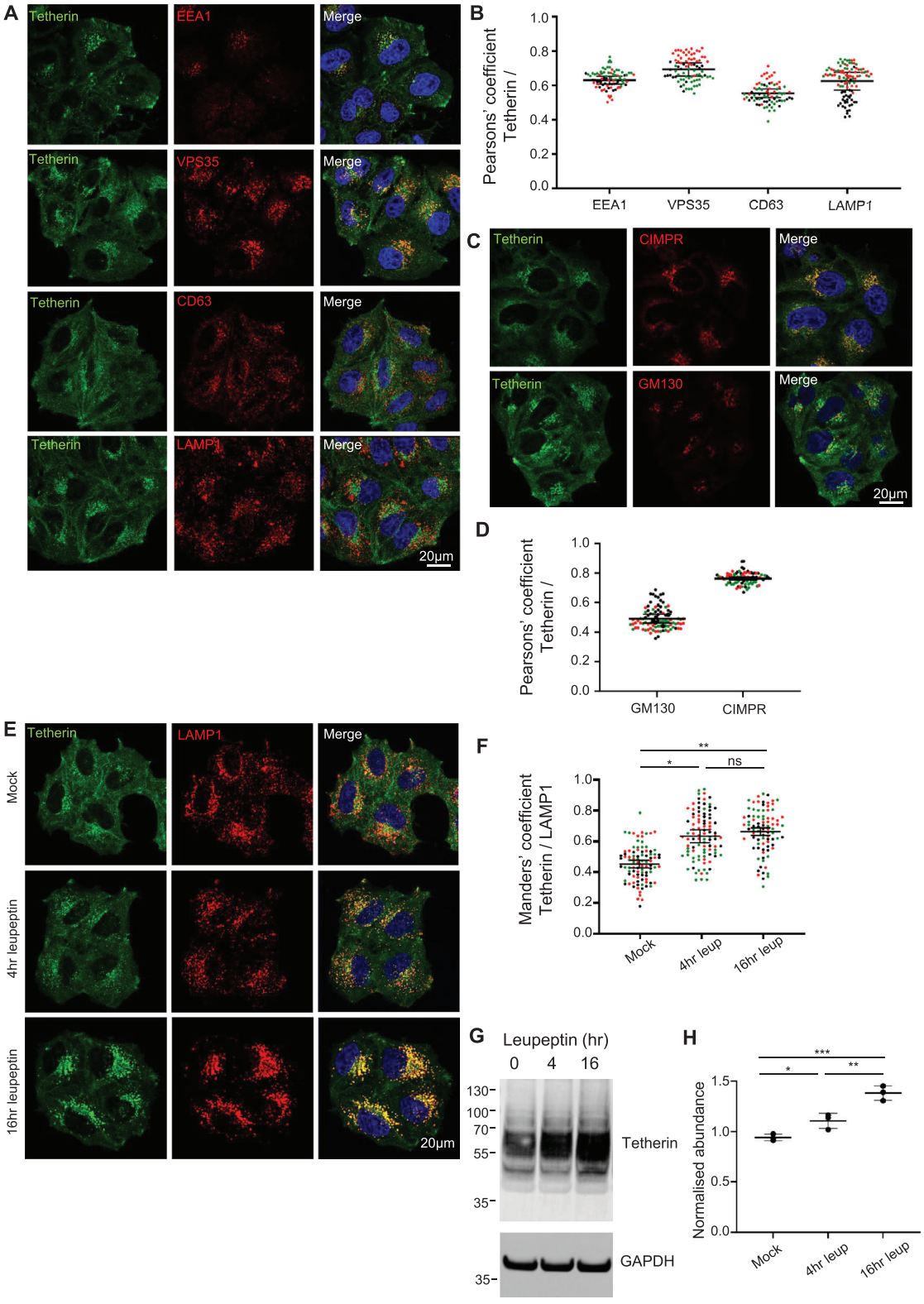


FIGURE 1 | (A) Representative confocal images showing colocalisation of tetherin with endosomal markers in WT HeLa cells, stained with DAPI (blue), anti-tetherin (green) and one of the following endosomal markers (red): EEA1 (early endosomes), VPS35 (retromer complex), CD63 (late endosomes/MVBs) or LAMP1 (lysosomes). Scale bars, 20 μm. (B) Quantification of colocalisation between tetherin and endosomal markers. Pearsons' correlation coefficients between tetherin and the endosomal markers EEA1, VPS35, CD63 and LAMP1 in WT HeLa cells. Data represent three independent biological replicates ($n > 74$ cells), each dot corresponds to an individual cell; red, green and black colours represent separate biological replicates. Bars indicate mean ± SEM. Mean values: tetherin/EEA1 = 0.28 ± 0.06; tetherin/VPS35 = 0.42 ± 0.07; tetherin/CD63 = 0.21 ± 0.03; tetherin/LBPA = 0.18 ± 0.03; tetherin/LAMP1 = 0.34 ± 0.06. (C) Representative confocal images showing colocalisation of tetherin with biosynthetic pathway markers in WT HeLa cells, stained with DAPI (blue), anti-tetherin (green) and either GM130 (Golgi apparatus) or CIMPR (trans-Golgi network/early endosomes) (red). Scale bars = 20 μm. (D) Quantification of colocalisation between tetherin and biosynthetic pathway markers.

as rescue cell lines, ectopically expressed in Bst2KO HeLa cells. Each construct was engineered with a haemagglutinin (HA) epitope inserted into the luminal domain, facilitating downstream analysis and eliminating dependence on anti-tetherin antibodies, which may not bind all mutants with equal affinity. The addition of the HA tag has been shown to minimally impact tetherin function (Billcliff et al. 2013), and Bst2-HA expression has previously been demonstrated to restore exosome tethering (Edgar et al. 2016; Palmulli et al. 2025). We established the following rescue cell lines, all of which were expressed in Bst2KO background:

1. **+Bst2-HA**: Wild-type human tetherin, modified only by the addition of the HA epitope inserted within the extracellular domain.
2. **+C3A-HA**: A mutant in which three evolutionarily conserved cysteine residues within the coiled-coil domain are replaced with alanine. These cysteine residues are essential for tetherin homodimerisation, and their mutation disrupts the ability to tether HIV-1 (Perez-Caballero et al. 2009), SARS-CoV-2 (Stewart et al. 2023) and midbody remnants (Presle et al. 2021).
3. **+K18A-HA**: Mutation of the single lysine residue in the N-terminal, short cytosolic domain. This lysine residue is targeted by Kaposi's sarcoma-associated herpesvirus ubiquitin ligase K5, and its ubiquitination enhances tetherin trafficking to endosomes and lysosomes in an ESCRT-dependent manner (Pardieu et al. 2010).
4. **ΔNterm-HA**: Deletion of the N-terminal cytosolic domain, including the YXXΦ endocytic motif and K18.
5. **ΔGPI-HA**: Introduction of a premature stop codon prevents the generation of the GPI anchor. The GPI promotes tetherin's localisation to cholesterol-rich domains (Billcliff et al. 2013).

Schematics of endogenous tetherin and HA-tagged rescue constructs are shown in Figure 2B.

Stable expression of these constructs was confirmed by immunofluorescence microscopy (Figure 2C), Western blotting (Figure 2D, Figure S2A) and flow cytometry (Figure 2E, Figure S2B). In nonreducing conditions, tetherin appeared as a homodimer on Western blots (Figure 2D), confirming the loss of homodimer formation upon expression of +C3A-HA. As expected, reduction of cell lysates abolished dimer formation by cleaving disulfide bonds (Figure S2A). All rescue constructs localised to some degree to the plasma membrane, to a perinuclear region and to cytosolic puncta, as shown by endogenous tetherin (Figure 1A–D). However, the expression of +C3A-HA displayed enhanced plasma membrane localisation (Figure 2C,E), consistent with previous reports (Presle et al. 2021). Flow cytometry analysis using anti-tetherin antibodies suggested reduced surface C3A; however, the anti-tetherin antibody is raised against the extracellular domain of tetherin and so may have reduced affinity for C3A tetherin (Figure 2E). Indeed, analysis using anti-HA antibodies demonstrates relative equal surface levels of all rescue constructs. We compared the extent of HA colocalisation with VPS35 (Figure 2F)—the endosomal marker that showed the highest level of colocalisation with tetherin (Figure 1A,B)—between +Bst2-HA and +C3A-HA cells and observed a significant reduction in +C3A-HA association with endosomes relative to +Bst2-HA (Figure 2G).

Next, we analysed the impact of tetherin mutation on exosome tethering. Transmission electron microscopy was performed on cells to examine the capacity of each cell line to retain exosomes at their plasma membrane (Figure 3A, Figure S3A). The propensity of MVB fusion with the plasma membrane was increased by treating cells with Bafilomycin A1 (Edgar et al. 2016; Mathieu et al. 2021). Exosomes were frequently observed as clumps closely associated to the plasma membrane (Figure S3A) from a number of cell lines, and clathrin-coated vesicles were frequently observed that contained multiple exosomes (Figure S3B). The frequency of exosomes at the plasma membranes of cells was quantified (Figure 3B) and revealed that expression of +Bst2-HA, +K18A-HA and +ΔNterm-HA restored exosome tethering to levels comparable to wild-type tetherin. In contrast, +C3A-HA expression significantly impaired exosome retention, with a frequency similar to that observed in Bst2KO cells. Cells expressing ΔGPI-HA showed a partial rescue, with more exosomes at the plasma membrane than in Bst2KO or +C3A-HA cells, but fewer than in wild-type or other functional rescue lines.

Pearsons' correlation coefficients between tetherin and GM130 or CIMPR in WT HeLa cells. Data represent three independent biological replicates (n > 82 cells), each dot corresponds to an individual cell; red, green and black colours represent separate biological replicates. Bars indicate mean ± SEM. Mean values: tetherin/GM130 = 0.08 ± 0.02; tetherin/CIMPR = 0.38 ± 0.06. (E) Representative confocal images showing colocalisation of tetherin and LAMP1 following leupeptin treatment in WT HeLa cells. Cells were incubated with 50 μg/mL leupeptin for 4 or 16 h, fixed and stained with DAPI (blue), anti-tetherin (green) and anti-LAMP1 (red) antibodies. Scale bars = 20 μm. (F) Quantification of colocalisation between tetherin and LAMP1 in WT HeLa cells following leupeptin treatment. Manders' correlation coefficients between tetherin and LAMP1 are shown. Data represent three independent biological replicates (n > 87 cells per condition), each dot represents an individual cell; red, green and black dots denote separate biological replicates. Bars indicate mean ± SEM. Mean values: mock = 0.45 ± 0.03; 4 h = 0.64 ± 0.04; 16 h = 0.66 ± 0.03. Statistical analysis was performed using ordinary one-way ANOVA followed by Tukey's multiple comparisons test. Mock versus 4 h (p = 0.0161), mock versus 16 h (p = 0.0081), 4 versus 16 h (p = 0.8046). p > 0.05 (ns), $p \leq 0.05$ (*), $p \leq 0.01$ (**), $p \leq 0.001$(***) and $p \leq 0.0001$ (****). (G) Representative Western blot of tetherin expression in WT HeLa cells following leupeptin treatment. WT HeLa cells were either untreated (mock) or incubated with 50 μg/mL leupeptin for 4 or 16 h. Total cell lysates were analysed by Western blotting using anti-tetherin antibodies in nonreduced conditions. GAPDH was used as a loading control. (H) Quantification of tetherin protein levels in mock WT HeLa cells, or cells treated with leupeptin (4 or 16 h). Tetherin abundance was assessed by Western blotting and normalised to GAPDH. Each dot represents the normalised tetherin level from one independent experiment (n = 3). Bars indicate mean ± SEM (mock = 1.03 ± 0.02, 4 h = 1.21± 0.05, 16 h = 1.52 ± 0.05). Statistical analysis was performed using one-way ANOVA with Tukey's multiple comparisons test. p > 0.05 (ns), $p \leq 0.05$ (*), $p \leq 0.01$ (**), $p \leq 0.001$(***) and $p \leq 0.0001$ (****). Mock versus 4 h leupeptin (p = 0.0445), mock versus 16 h leupeptin (p = 0.0004).

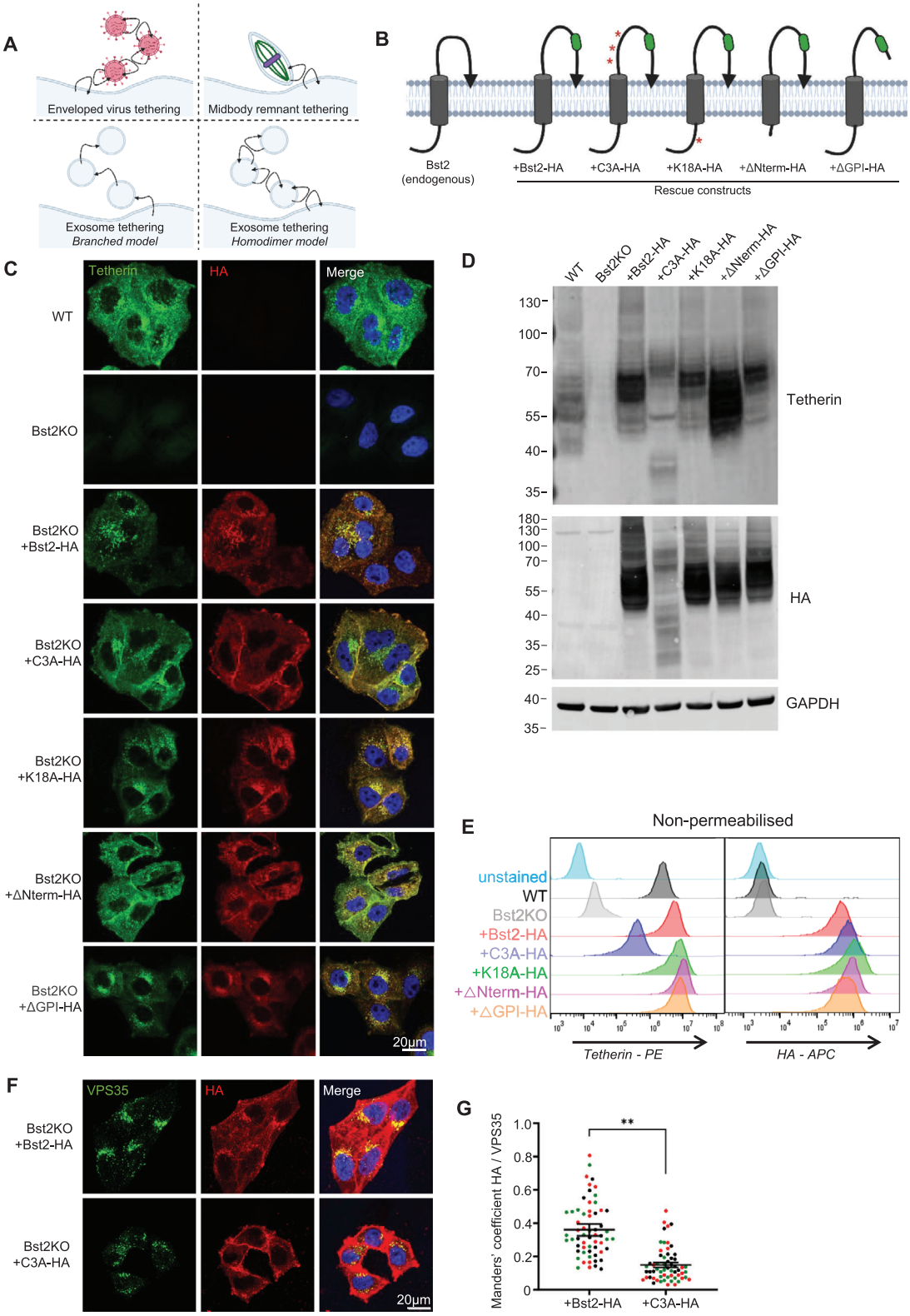


FIGURE 2 | (A) Schematic model tetherin-dependent tethering of enveloped viruses (top left), midbody remnants (top right) and potential mechanisms of exosome tethering (bottom). (B) Diagram of tetherin membrane topology and rescue constructs. Point mutations are indicated by red asterisks, and HA tag by green square. (C) Confocal immunofluorescence images of WT, Bst2KO and -HA rescue HeLa cells stably expressing: +Bst2-HA, +C3A-HA, +K18A-HA, +ΔNterm-HA and +ΔGPI-HA, stained with anti-tetherin (green) and anti-HA (red) antibodies, and DAPI (blue). Scale bars = 20 μm. Representative images from three independent biological experiments. (D) Western blot analysis of WT, Bst2KO and -HA rescue HeLa cells stably expressing: +Bst2-HA, +C3A-HA, +K18A-HA, +ΔNterm-HA and +ΔGPI-HA. Samples were run in nonreducing conditions (-DTT) to preserve tetherin dimerisation. Blots were probed with anti-tetherin, anti-HA and anti-GAPDH (loading control) antibodies. (E) Flow cytometry analysis of surface tetherin expression WT, Bst2KO and -HA rescue lines using anti-tetherin and anti-HA antibodies. (F) Confocal images of +Bst2-HA

To complement this data, we examined the ability of these cells to release exosomes. Exosome-enriched preparations were isolated from conditioned media of each cell line and analysed by Western blotting (Figure 3C,D, Figure S3C, D). The relative enrichment of the exosome-enriched proteins CD63, ALG-2 interacting protein X (ALIX), Tsg101 and syntenin, and the relative de-enrichment of cellular markers GAPDH and GM130 confirmed the successful enrichment of exosomes. Western blot analysis showed that none of the mutations impaired tetherin's ability to traffic to exosomes, as both tetherin and -HA were present in the exosome-enriched fractions from all rescue cell lines. The levels of the exosome-enriched proteins, CD63, ALIX, Tsg101 and syntenin were elevated in preparations from Bst2KO and +C3A-HA cell lines. Quantification confirmed a statistically significant increase in exosome release between WT and Bst2KO, and also between +Bst2-HA and +C3A-HA cells (Figure 3C,D, Figure S3D).

Nanoparticle analysis was performed to quantify EV particle concentrations released by each cell line (Figure 3E). Consistent with our biochemical data, Bst2KO and +C3A-HA cells released significantly more EVs, whereas expression of +K18A-HA, +Nterm-HA or +GPI-HA reduced particle concentrations to levels comparable to WT or +WT-HA cells. The purity of our EV factions was analysed using DAISY analysis, which allows particle-by-particle determination of both size and refractive index (Olsén et al. 2024). This makes it possible to detect and quantify subpopulations within heterogenous particle mixtures. Of particular relevance for EV studies is the identification of possible lipoprotein contaminants within samples and determination of aggregate formation, both of which can significantly alter observed particle concentrations. As a control for sample purity and consistency, we applied DAISY analysis to the EV fractions derived from our cell lines. DAISY analysis showed our samples to be consistent, with the bulk of particles having a refractive index of below 1.4 (EV reference samples have been assessed by DAISY to have refractive index <1.4 while lipoproteins have a refractive index >1.4). This increases confidence in our observed particle concentrations (Figure S3E).

Our data suggested that disulfide bonds between tetherin molecules are essential for exosome tethering; however, it remained possible that the C3A mutations impaired exosome tethering through an alternative mechanism. To test whether cysteine-linked homodimer formation of tetherin molecules is sufficient for exosome tethering, we generated a novel tetherin rescue construct—termed Forced Dimer (FD)—that lacked Cys53, Cys63 and Cys91 (as in C3A), but incorporated additional cysteine residues at positions 78, 86 and 141 (Figure S4A). These positions were selected based on previous studies identifying them as permissive sites to drive tetherin homodimer formation biochemically (Welbourn et al. 2015). The FD construct expressed, acted as a homodimer biochemically (Figure S4B) and localised similarly to Bst2-HA (Figure S4C). Analysis of exosome-enriched fractions showed that FD tetherin tethered exosomes less efficiently than Bst2-HA, but slightly more effectively than the homodimer-incompatible C3A-HA mutant (Figure S4D). Quantification of exosome tethering by electron microscopy verified the partial ability of FD cells to rescue exosome tethering.

Together, these data demonstrate that exosome release is increased by tetherin depletion, and that effective exosome tethering requires expression of homodimer-competent tetherin.

3.3 | Tetherin Is Trafficked to ILVs Irrespective of Ubiquitination, Its GPI-Anchor or ESCRT-0 Recruitment

In order for tetherin to tether exosomes, it must first be trafficked to ILVs of MVBs. We previously demonstrated that endogenous tetherin localises to the ILVs of MVBs (Edgar et al. 2016), but how tetherin is trafficked to ILVs, and whether it traffics to all subtypes of ILVs (and subsequently exosome subtypes) remains unclear.

Tetherin has two prominent features that could promote its traffic to ILVs: a cytosolic lysine residue (Lysine18), which is a target for ubiquitination (Mansouri et al. 2009), and a C-terminal GPI anchor. Both ubiquitination (Migliano and Teis 2018) and the presence of GPI anchors (MacDonald et al. 2015) promote the traffic of cargos to ILVs.

Although a proportion of endogenous tetherin recycles from endosomes to the biosynthetic pathway (Stewart et al. 2023), the mechanism determining whether tetherin remains on the limiting endosomal membrane or is sorted into ILVs are unclear. Ubiquitination of Lysine18 drives tetherin towards ILVs, as demonstrated by the effects of the KHSV ubiquitin ligase K5 (Mansouri et al. 2009).

Cryo immunogold electron microscopy provides the ultrastructural resolution and required immunolabelling resolution to differentiate the limiting membrane of endosomes from the ILVs. Immunogold electron microscopy was performed on Bst2-HA, K18-HA and GPI-HA cell lines, and the localisation of each protein was analysed using anti-HA antibodies. Consistent with prior data, Bst2-HA localised to ILVs (Edgar et al. 2016). Surprisingly, neither mutation of K18 or loss of the GPI anchor impacted tetherin localisation to ILVs (Figure 4A).

ILVs can be generated by a number of potential different molecular mechanisms. The ESCRT machinery is the best-described mechanism and utilises a conserved pathway of over 30 proteins to recognise and bind cargos, concentrate them to domains on the endosome limiting membrane, and subsequently drive the inward vesiculation of the limiting membrane, resulting in ILV formation. Given different populations of ILVs exist and traffic different cargos (Edgar et al. 2014; Stuffers et al. 2009; van

and +C3A-HA rescue HeLa cells stained with anti-VPS35 (green), anti-HA (red) and DAPI (blue). Scale bar = 20 μm. Representative images from three independent biological experiments. (G) Quantification of colocalisation between HA-tagged tetherin constructs and VPS35 in +Bst2-HA or +C3A-HA rescue HeLa cells using Manders' correlation coefficients. Each dot represents an individual cell ($n = 20$ per condition); red, green and black dots represent independent biological experiments. Bars indicate mean ± SEM (+WT-HA; 0.36 ± 0.01, C3A-HA; 0.15 ± 0.01). Statistical significance was assessed using an unpaired two-tailed *t* test; $p > 0.05$ (ns), $p \leq 0.05$ (*), $p \leq 0.01$ (**), $p \leq 0.001$(***) and $p \leq 0.0001$ (****).

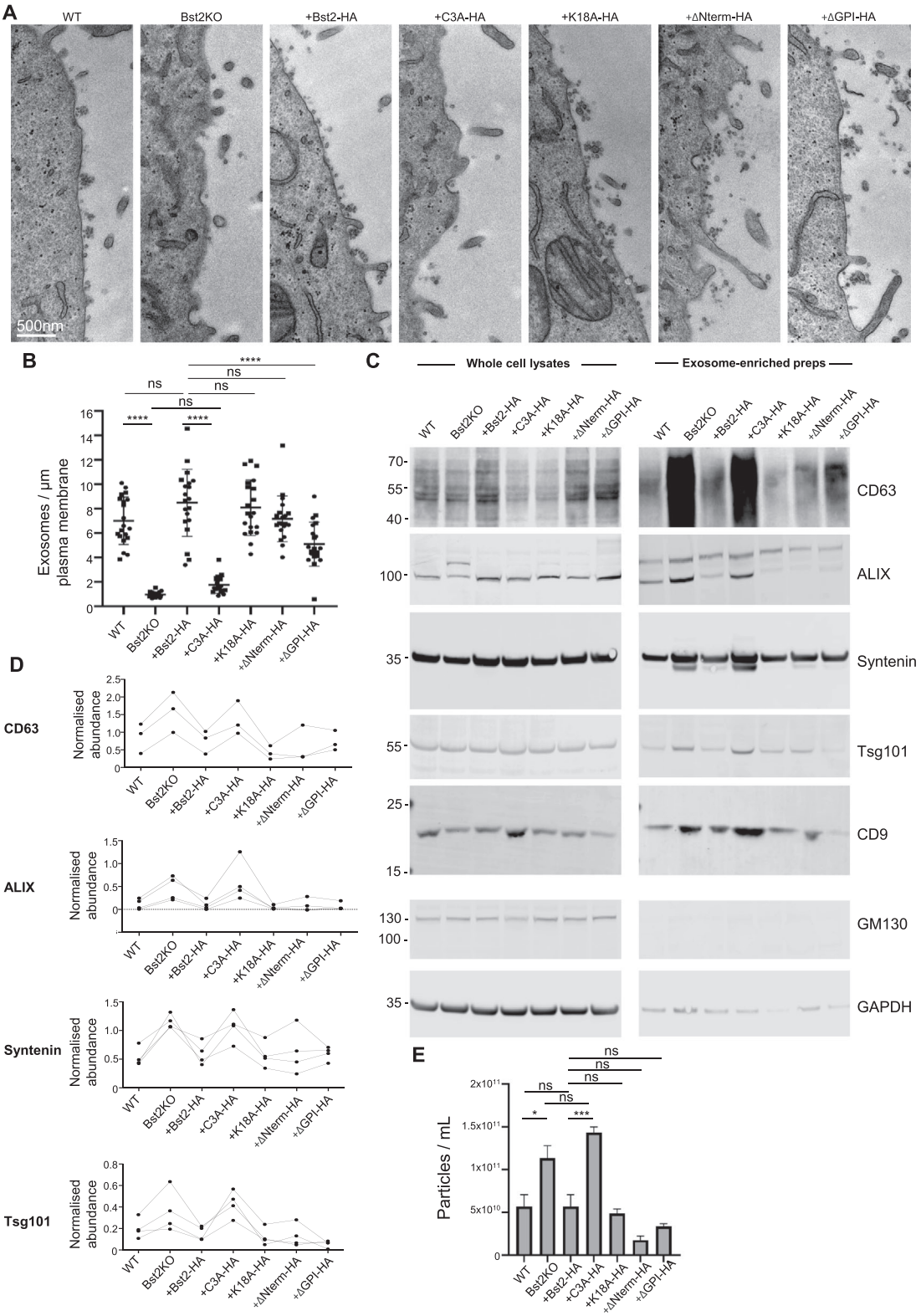


FIGURE 3 | (A) Conventional transmission electron microscopy of WT, Bst2KO and tetherin-HA rescue HeLa cell lines that were treated with Bafilomycin A1 (100 nM, 16 h) to induce exosome release. Scale bar = 500 nm. (B) The frequency of exosomes at the plasma membrane of cells was quantified. Data show the average number of exosomes/µm plasma membrane. Each data point represents an individual cell. n = two independent biological experiments, and for each independent experiment, at least two separate ultrathin sections were analysed. Bars indicate mean ± SD. Mean values: WT = 7.01 ± 1.94; KO = 0.70 ± 0.23; Bst2-HA = 8.48 ± 2.75; C3A-HA = 1.75 ± 0.68; K18A-HA = 8.09 ± 2.27; ΔNterm-HA = 7.17 ± 1.88; ΔGPI-HA = 5.10 ± 1.81. Statistical analysis was performed using one-way ANOVA with Tukey's multiple comparisons test. $p > 0.05$ (ns), $p \leq 0.05$ (*), $p \leq 0.01$ (**), $p \leq 0.001$(***) and $p \leq 0.0001$(****). WT versus KO ($p < 0.0001$), WT versus Bst2-HA ($p = 0.1560$), KO versus C3A-HA ($p = 0.8316$), Bst2-HA versus KO ($p < 0.0001$), Bst2-HA versus C3A-HA ($p < 0.0001$), Bst2-HA versus K18A-HA ($p = 0.9935$), Bst2-HA versus ΔNterm-HA ($p = 0.2785$), Bst2-HA versus ΔGPI-HA ($p < 0.0001$). Standardised effect size: ANOVA $\omega^2 = 0.70$. Effect sizes (Cohen's d): WT versus KO (4.37), WT versus Bst2-HA (0.62), KO versus

Niel et al. 2011), it is likely that different exosome populations also exist. As a result, tetherin-positive ILVs/exosomes may be tethered, whilst tetherin-negative ILVs/exosomes may be released freely from cells.

To examine whether tetherin was trafficked to ILVs/exosomes in an ESCRT-dependent manner, and whether ESCRT depletion altered exosome fate, cells were depleted of the ESCRT-0 protein, Hrs (Figure 4B) and the localisation of endogenous tetherin analysed by immunogold electron microscopy (Figure 4C). Endosome enlargement and the formation of small ILVs, both characteristic of Hrs depletion (Edgar et al. 2014), were observed. Endogenous tetherin localised to ILVs in Hrs-depleted cells, demonstrating that its traffic to ILVs is not solely dependent upon Hrs, and that its traffic to ILVs is not solely ESCRT-dependent.

To analyse the impact of Hrs loss on exosome tethering, we hoped to analyse exosome release biochemically. However, Hrs-depleted cells displayed defects in cell division (likely due to Hrs' requirement for cytokinesis). Instead, we analysed endosome traffic and exosome release using immunofluorescence and ultrastructural analysis. Immunofluorescence microscopy demonstrated that CD63+ endosomes remained intracellular in Hrs-depleted cells and failed to relocalise to the plasma membrane upon induction with Bafilomycin A1 (Figure 4D, Figure S5A). Endosomes appeared to cluster at the perinuclear region of cells in Hrs-depleted cells, irrespective of treatment with Bafilomycin A1 (Figure S5A, B). The induction of exosome release by Bafilomycin A1 has become a useful tool to study exosome release (Mathieu et al. 2021), and exosome tethering can be readily observed in mock cells treated with Bafilomycin A1 (Figure S5C). However, Hrs-depleted cells treated with Bafilomycin A1 did not display tethered exosomes, and instead MVBs could frequently be observed adjacent to the plasma membrane (Figure S5C), indicating that Hrs-depleted MVBs were impaired in their ability to fuse with the plasma membrane.

3.4 | Live-Cell Imaging Reveals Functional Tetherin Impacts Exosome Persistence

Although we demonstrated the presence of tetherin in endosomes and ILVs, and the functional consequences of tetherin loss or mutation, we wanted to determine whether we could visualise tetherin at sites of exosome release. To achieve this, we generated mScarlet-tagged tetherin constructs and expressed these ectopically in MelJuSo cells. MelJuSo cells are widely used to study exosome release (Perrin et al. 2021), and release exosomes at steady state and without the requirement for induction via Bafilomycin A1, which would prohibit the use of CD63-pHlourin. MelJuSo cells do not express detectable levels of tetherin at steady state and so were incubated with interferon to induce tetherin expression. We stably expressed either Bst2-mScarlet or C3A-mScarlet in Bst2KO MelJuSo cells (Figure 5A) and verified the expression of tetherin and mScar expression by flow cytometry (Figure 5B) and immunofluorescence microscopy (Figure 5C). Stable expression of Bst2-mScar or C3A-mScar in Bst2KO MelJuSo cells produced mScarlet fluorescence patterns that were consistent with the localisation of both endogenous and ectopically expressed HA-tagged tetherin, as previously observed (Figures 1A and 2C).

Western blot analysis of whole cells confirmed the expression of both constructs, demonstrating that while Bst2-mScar retained the ability to form homodimers, C3A-mScar could not (Figure 5D). The functionality of mScar constructs was explored biochemically, and Bst2-mScar cells were found to be able to tether exosomes in a manner similar to WT cells, and C3A-mScar cells found to be unable to tether exosomes (Figure 5D, Figure S6A, B) as previously demonstrated (Figure 3A–D).

Analogous experiments were performed in HeLa cells where Bafilomycin A1 was used to induce exosome release. The expression of mScar constructs (Figure S7A–C) and ability to tether exosomes (Figure S7D, E) confirmed the ability of Bst2-mScar, but not C3A-mScar, to tether exosomes. Transmission electron microscopy of HeLa cell lines also confirmed the presence of tethered exosomes from WT and Bst2-mScar cells, but with greatly reduced frequency in Bst2KO and C3A-mScar cells (Figure S7F), consistent with our earlier findings using -HA-tagged tetherin (Figure 3A–E, Figure S3A–D).

Bst2- or C3A-mScar-expressing MelJuSo cells were transiently transfected with CD63-pHluorin, a reporter that enables visualisation of MVB-plasma membrane fusion and subsequent exosome release to be imaged (Verweij et al. 2018) using TIRF microscopy. CD63-pHluorin signal was detected together with Bst2- or C3A-mScar signal, confirming that these constructs localise to MVBs undergoing fusion with the plasma membrane (Figure 5E). To assess exosome retention, we compared the kinetics of CD63-pHluorin persistence between tethering-competent Bst2-mScar and tethering-incompetent C3A-mScar cells. Quantification of CD63-pHlourin signal persistence revealed a significant reduction in signal persistence in C3A-mScar cells

Bst2-HA (3.85), Bst2-HA versus C3A-HA (3.36), Bst2-HA versus K18A-HA (0.16), Bst2-HA versus ΔNterm-HA (0.56), Bst2-HA versus ΔGPI-HA (1.46). (C) Whole cell lysates and exosome-enriched preparations were isolated from WT, Bst2KO and tetherin-HA rescue HeLa cell lines. Western blotting was performed and probed with antibodies against exosome-enriched proteins CD63, ALIX, Syntenin, Tsg101, CD9 and the EV-negative marker GM130 and loading control (GAPDH). Data representative of three independent biological experiments. (D) Western blots were analysed, and protein abundance was normalised to loading controls. Relative abundance for exosome-enriched markers are shown. (E) Quantification of particles using nanoparticle tracking analysis (NTA) was performed (Zetaview). Particle concentrations are shown as particles/mL. Analysis was performed using the ZetaView system across 11 positions per sample, with ≥1000 completed tracks per condition to ensure robust quantification, and three independent biological experiments were performed. Bars indicate mean ± SEM. Statistical analysis was performed using one-way ANOVA with Tukey's multiple comparisons test. $p > 0.05$ (ns), $p \leq 0.05$ (*), $p \leq 0.01$ (**), $p \leq 0.001$(***) and $p \leq 0.0001$(****). WT versus KO ($p = 0.0163$), WT versus Bst2-HA ($p > 0.9999$), KO versus C3A-HA ($p = 0.377$), Bst2-HA versus C3A-HA ($p = 0.0004$), Bst2-HA versus K18A-HA ($p = 0.9959$), Bst2-HA versus ΔNterm-HA ($p = 0.1395$), Bst2-HA versus ΔGPI-HA ($p = 0.6433$). Standardised effect size: ANOVA $\omega^2 = 0.88$. Effect sizes (Cohen's d): WT versus KO (2.31), WT versus Bst2-HA (0.00), KO versus Bst2-HA (2.31), Bst2-HA versus C3A-HA (4.66), Bst2-HA versus K18A-HA (0.47), Bst2-HA versus ΔNterm-HA (2.24), Bst2-HA versus ΔGPI-HA (1.37).

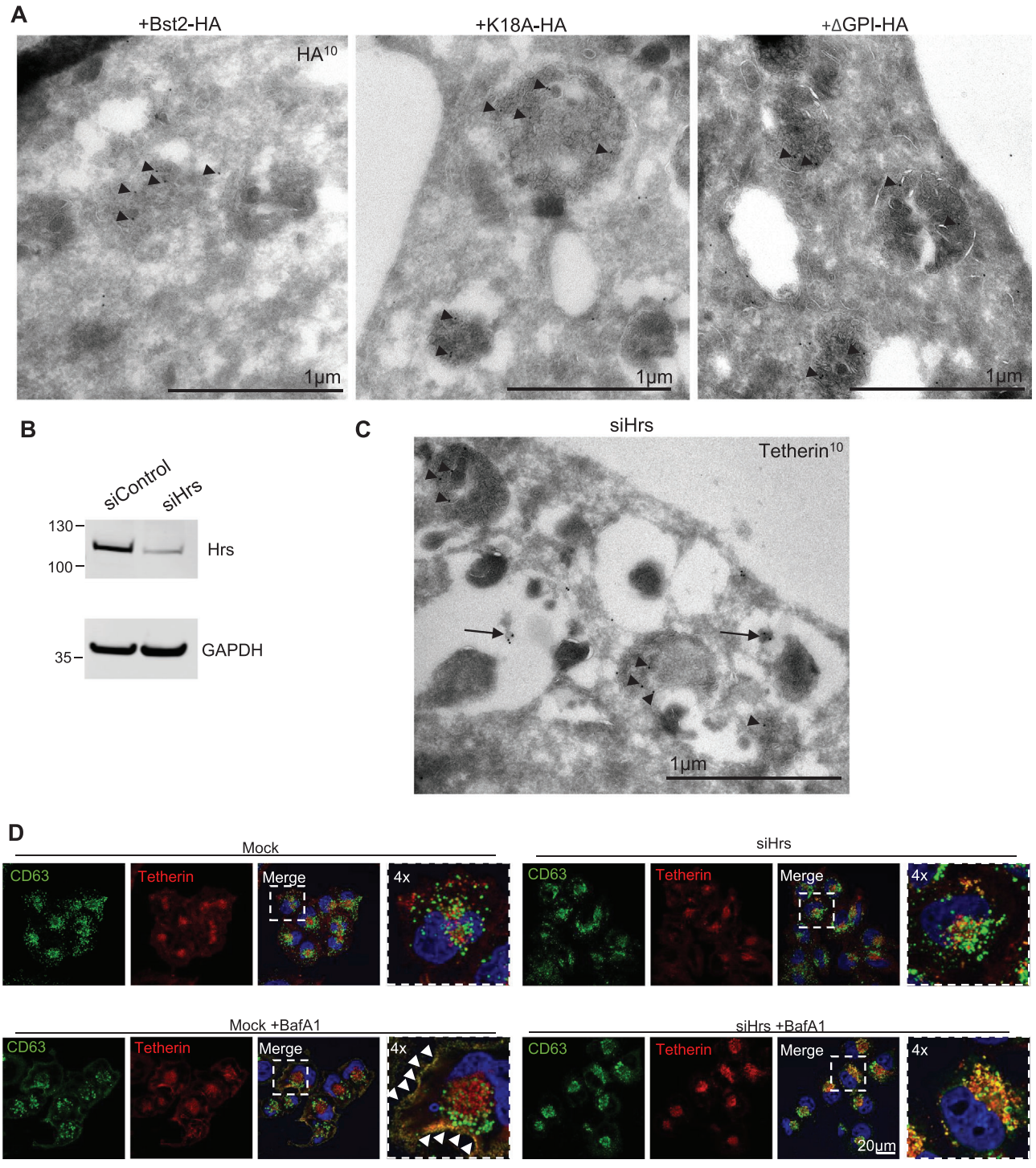


FIGURE 4 | (A) Cryoimmunogold electron microscopy was performed on + Bst2-HA, +K18A-HA or +GPI-HA rescue cell lines. Ultrathin sections were cut, collected and stained with anti-HA antibodies and protein-A gold 10 nm. Scale bar = 1 μm. (B) WT HeLa cells treated with either control or Hrs-targeting siRNA. Mock and Hrs-depleted whole cell lysates were blotted for Hrs to determine its protein abundance. GAPDH is used as a loading control. Representative blots shown (from at least three biologically independent experiments). (C) Cryoimmunogold electron microscopy was performed on Hrs-depleted WT HeLa cells. Ultrathin sections were cut, collected and stained with anti-tetherin antibodies and protein-A gold 10 nm. Scale bar = 1 μm. (D) WT HeLa cells were depleted for Hrs using siRNA. Mock or Hrs-depleted cells were plated to coverslips and treated without or with Bafilomycin A1 (100 nM, 16 h) before fixation and immunofluorescence. Cells were stained using anti-CD63 (green), anti-tetherin (red) and DAPI (blue). Arrowheads highlight plasma membrane localisation of CD63 and tetherin. Scale bar = 20 μm, and 4x magnification shown.

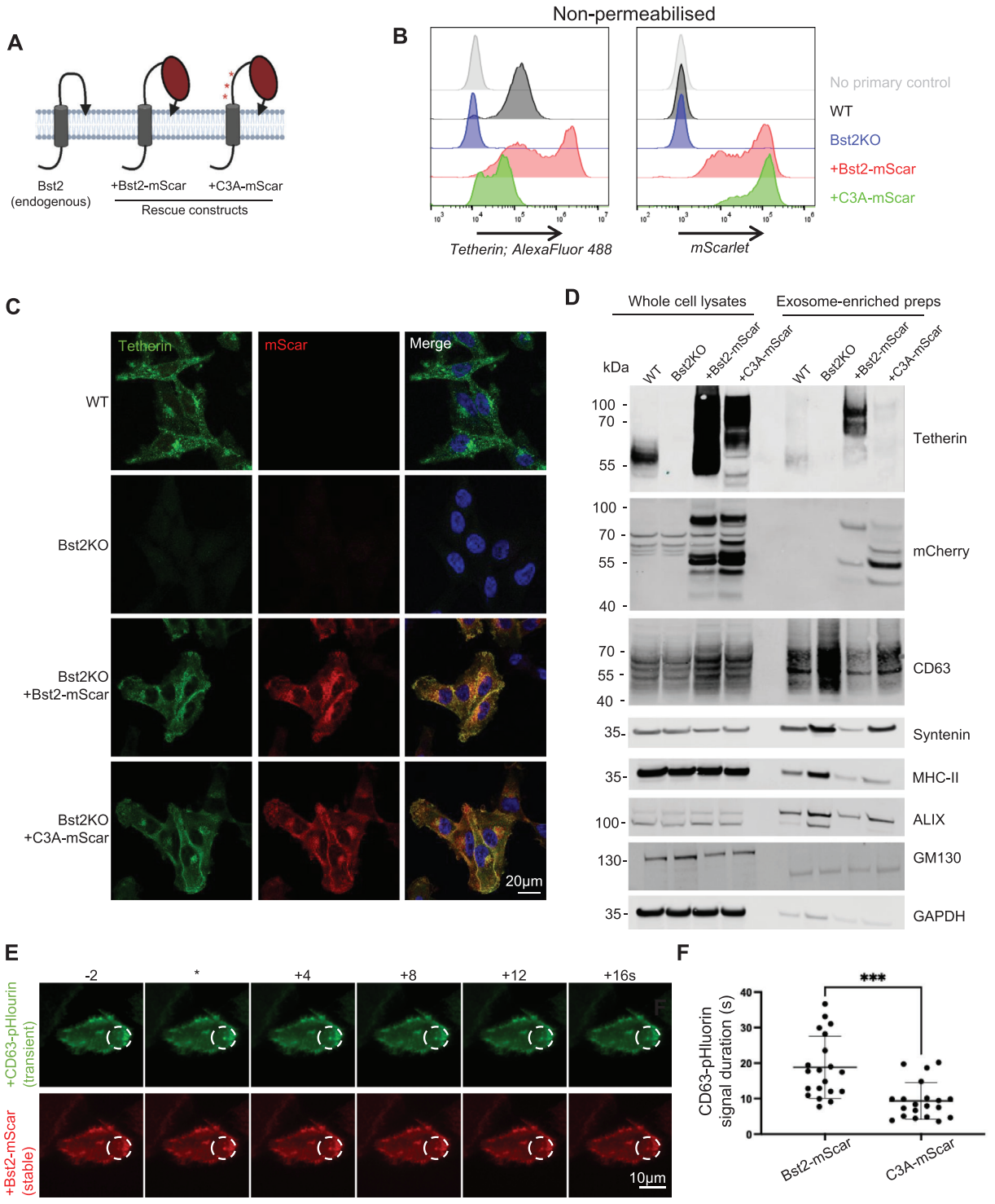


FIGURE 5 | (A) Diagram of tetherin membrane topology and -mScar rescue constructs. Point mutations within C3A-mScar are indicated by red asterisks. (B) Flow cytometry analysis of WT, Bst2KO, Bst2KO +Bst2-mScar and +C3A-mScar MelJuSo cells. Cells were treated with interferon gamma (100 ng/mL) to promote tetherin expression. Surface tetherin (rabbit, unconjugated antibody) expression and mScarlet levels were analysed. WT cells without antibody staining were used as a no primary control. (C) WT, Bst2KO, +Bst2-mScar and +C3A-mScar MelJuSo cells were analysed by immunofluorescence microscopy. Cells were stained with anti-tetherin (green) antibodies and DAPI (blue). Cells were treated with interferon gamma (100 ng/mL) to promote tetherin expression. (D) Exosome-enriched preparations were generated from WT, Bst2KO, +Bst2-mScar and +C3A-mScar MelJuSo cells. Whole cell lysates and exosome-enriched preparations were analysed by Western blot and probed with anti-tetherin, anti-mCherry antibodies. The exosome-enriched proteins CD63, Syntenin, MHC-II and ALIX were analysed, as were the negative control and loading controls, GM130 and GAPDH. (E) +Bst2-mScar MelJuSo cells were transiently transfected with CD63-pHlourin. Total internal reflection microscopy was performed. Stills from movies are shown before, upon (*) and following the generation of CD63-pHlourin bursts. (F) The mean duration of CD63-pHluorin was calculated and shown. $n = 20$ total cells analysed, from 6 independent biological experiments. Bars indicate mean ± SD (Bst2-mScar: 18.99 ± 8.72; C3A-mScar: 9.33 ± 5.18). Statistical significance was assessed using an unpaired two-tailed t test; $p > 0.05$ (ns), $p \leq 0.05$ (*), $p \leq 0.01$ (**), $p \leq 0.001$(***) and $p \leq 0.0001$ (****).

(Figure 5F). These findings further indicate that functional tetherin impacts the kinetics of exosome release.

4 | Discussion

Although exosomes and other extracellular vesicles can be isolated from biofluids and from conditioned media, their retention at the surface of producer cells highlights previously underappreciated functions. Although much research has explored the functions of released exosomes, very few studies have investigated surface-tethered exosomes. This may in part by due to their recent discovery and the requirement for ultrastructural imaging to visualise tethered exosomes. A number of seminal exosome studies utilise transmission electron microscopy to demonstrate the presence of exosomes, and in many published images exosomes appear clustered and clumped (Carroll-Portillo et al. 2012; Colombo et al. 2014; Edgar 2016; Johnstone 1992; Möbius et al. 2002; Raposo and Stoorvogel 2013; Raposo et al. 1996; Stoorvogel et al. 2002)—reminiscent of tetherin-dependent tethered exosomes.

Our data demonstrate that exosome tethering requires the formation of cysteine-linked tetherin homodimers (Figure 3A–D)—a feature also required for the tethering of both enveloped viruses and midbody remnants. The loss of the N-terminus or mutation of the sole cytosolic lysine residue had no impact on the ability of tetherin to traffic to endosomes (Figure 2C), ILVs (Figure 4A), exosomes (Figure S3C, D) or their ability to tether exosomes (Figure 3A–D). Loss of the GPI-anchor did not impact tetherin traffic to endosomes (Figure 2C), traffic to ILVs (Figure 4A) or exosomes (Figure S3C, D), but did functionally reduce its ability to retain exosomes (Figure 3A–D), consistent with the impact on virus tethering where GPI-lacking tetherin is impaired in its ability to restrict virions (Neil et al. 2008).

Exosome tethering impairs exosome release. The fate and kinetics of tethered exosomes is likely to differ between cell types relating to the relative dynamics of plasma membrane turnover. In this study, we frequently observed clusters of exosomes within clathrin-coated vesicles, consistent with their re-endocytosis upon retention at the plasma membrane (Figure S3B). We also demonstrated that functional tetherin prolongs the exposure of exosomes at the cell surface (Figure 5E,F). Released exosomes are also likely endocytosed by neighbouring cells, although we were unable to find example of vesicles within clathrin-coated vesicles from Bst2KO or C3A-HA cells. The relative rates of endocytosis by cells, and dynamics of plasma membrane remodelling likely impact the reabsorption of exosomes. Indeed, both enveloped viruses (Mitchell et al. 2009) and midbody remnants (Presle et al. 2021) are reabsorbed by cells in a tetherin-dependent manner, demonstrating that tetherin not only prevents particle escape from cells but also promotes its reinternalisation.

This redistribution may reflect the impact of tetherin monomerisation on its internalisation. We hypothesise that homodimers are internalised more efficiently than monomers, as the presence of dual domains may enhance engagement with the endocytic machinery, promoting uptake of the entire complex. In contrast, monomeric tetherin likely requires each individual molecule to independently interact with endocytic adaptors, potentially reducing the overall rate of internalisation.

Our data show that tetherin is trafficked to ILVs in the absence of cytosolic lysine or GPI-anchor (Figure 4A), and even in the absence of the ESCRT-0 component, Hrs (Figure 4C). Tetherin is trafficked through the endocytic pathway, and although it can undergo retrograde retrieval to the Golgi (Stewart et al. 2023), a proportion of tetherin remains in the endolysosomal pathway and is trafficked to late endosomes (Figure 1A,B). The tetherin positive late endosomes are not specifically fated for fusion with the plasma membrane with resultant formation of exosomes, as shown by the presence of tetherin in lysosomes and its accumulation upon treatment with Leupeptin (Figure 1E–H). Strikingly, we found that Hrs depletion impairs Bafilomycin A1-induced MVB-plasma membrane fusion and observed MVBs to be trafficked to the plasma membrane yet unable to fuse with it (Figure 4D, Figure S5A–C). Hrs depletion has been previously shown to reduce exosome secretion (Colombo et al. 2013). Our data highlight that exosome loss upon Hrs depletion may be due to impaired MVB-plasma membrane fusion in addition to the impairment of ESCRT-dependent ILV biogenesis.

Tetherin is antagonised by enveloped viruses through distinct mechanisms, most of which limit the localisation of tetherin from the respective site of viral budding. A number of viruses promote tetherin traffic to endosomes, including HIV-1 (Mitchell et al. 2009), Kaposi's sarcoma-associated herpesvirus (KSHV) (Mansouri et al. 2009) and SARS-CoV-2 (Stewart et al. 2023), which may promote tetherin levels on ILVs and subsequently exosomes. Viral antagonism of tetherin therefore may impact exosome fate, with implications for intracellular signalling and immune evasion.

Acknowledgements

We wish to thank the electron microscopy facility at the Cambridge Institute for Medical Research, University of Cambridge. The authors also gratefully acknowledge the Cambridge Microscopy Bioscience Platform for their support and assistance in this work, and thank the flow cytometry facility at the Department of Pathology, University of Cambridge.

Funding

James R. Edgar is supported by a Sir Henry Dale Fellowship jointly funded by the Wellcome Trust and the Royal Society (216370/Z/19/Z).

Conflicts of Interest

Paul T. Manna is an employee of Holtra AB. The other authors declare no conflicts of interest.

Data Availability Statement

Data generated or analysed during this study are available in the article and its online Supporting Information. Requests for materials should be addressed to James R. Edgar.

References

Billcliff, P. G., R. Rollason, I. Prior, D. M. Owen, K. Gaus, and G. Banting. 2013. "CD317/Tetherin Is an Organiser of Membrane Microdomains." *Journal of Cell Science* 126: 1553–1564.

Bobrie, A., M. Colombo, G. Raposo, and C. Théry. 2011. "Exosome Secretion: Molecular Mechanisms and Roles in Immune Responses." *Traffic (Copenhagen, Denmark)* 12: 1659–1668.

Bright, N. A., B. J. Reaves, B. M. Mullock, and J. P. Luzio. 1997. "Dense Core Lysosomes Can Fuse With Late Endosomes and Are Re-Formed From the Resultant Hybrid Organelles." *Journal of Cell Science* 110: 2027–2040.

Brown, D. A., and J. K. Rose. 1992. "Sorting of GPI-Anchored Proteins to Glycolipid-Enriched Membrane Subdomains During Transport to the Apical Cell Surface." *Cell* 68: 533–544.

Carroll-Portillo, A., Z. Surviladze, A. Cambi, D. S. Lidke, and B. S. Wilson. 2012. "Mast Cell Synapses and Exosomes: Membrane Contacts for Information Exchange." *Frontiers in Immunology* 3: 46.

Colombo, M., C. Moita, G. van Niel, et al. 2013. "Analysis of ESCRT Functions in Exosome Biogenesis, Composition and Secretion Highlights the Heterogeneity of Extracellular Vesicles." *Journal of Cell Science* 126: 5553–5565.

Colombo, M., G. Raposo, and C. Théry. 2014. "Biogenesis, Secretion, and Intercellular Interactions of Exosomes and Other Extracellular Vesicles." *Annual Review of Cell and Developmental Biology* 30: 255–289.

Edgar, J. R. 2016. "Q&A: What Are Exosomes, Exactly?" *BMC Biology* 14: 46.

Edgar, J. R., E. R. Eden, and C. E. Futter. 2014. "Hrs- and CD63-Dependent Competing Mechanisms Make Different Sized Endosomal Intraluminal Vesicles." *Traffic (Copenhagen, Denmark)* 15: 197–211.

Edgar, J. R., P. T. Manna, S. Nishimura, G. Banting, and M. S. Robinson. 2016. "Tetherin Is an Exosomal Tether." *eLife* 5: e17180.

Emmanouilidou, E., K. Melachroinou, T. Roumeliotis, et al. 2010. "Cell-Produced Alpha-Synuclein Is Secreted in a Calcium-Dependent Manner by Exosomes and Impacts Neuronal Survival." *Journal of Neuroscience* 30: 6838–6851.

Felder, S., K. Miller, G. Moehren, A. Ullrich, J. Schlessinger, and C. R. Hopkins. 1990. "Kinase Activity Controls the Sorting of the Epidermal Growth Factor Receptor Within the Multivesicular Body." *Cell* 61: 623–634.

Fevrier, B., D. Vilette, F. Archer, et al. 2004. "Cells Release Prions in Association With Exosomes." *Proceedings of the National Academy of Sciences of the United States of America* 101: 9683–9688.

Goldsmith, C. S., K. M. Tatti, T. G. Ksiazek, et al. 2004. "Ultrastructural Characterization of SARS Coronavirus." *Emerging Infectious Diseases* 10: 320–326.

Harding, C., J. Heuser, and P. Stahl. 1983. "Receptor-Mediated Endocytosis of Transferrin and Recycling of the Transferrin Receptor in Rat Reticulocytes." *Journal of Cell Biology* 97: 329–339.

Hirsch, J. G., M. E. Fedorko, and Z. A. Cohn. 1968. "Vesicle Fusion and Formation at the Surface of Pinocytic Vacuoles in Macrophages." *Journal of Cell Biology* 38: 629–632.

Hoshino, D., K. C. Kirkbride, K. Costello, et al. 2013. "Exosome Secretion Is Enhanced by Invadopodia and Drives Invasive Behavior." *Cell Reports* 5: 1159–1168.

Hurley, J. H., and P. I. Hanson. 2010. "Membrane Budding and Scission by the ESCRT Machinery: It's All in the Neck." *Nature Reviews Molecular Cell Biology* 11: 556–566.

Johnstone, R. M. 1992. "Maturation of Reticulocytes: Formation of Exosomes as a Mechanism for Shedding Membrane Proteins." *Biochemistry and Cell Biology = Biochimie et Biologie Cellulaire* 70: 179–190.

Kaletsky, R. L., J. R. Francica, C. Agrawal-Gamse, and P. Bates. 2009. "Tetherin-Mediated Restriction of Filovirus Budding Is Antagonized by the Ebola Glycoprotein." *Proceedings of the National Academy of Sciences of the United States of America* 106: 2886–2891.

Klein, S., M. Cortese, S. L. Winter, et al. 2020. "SARS-CoV-2 Structure and Replication Characterized by In Situ Cryo-Electron Tomography." *Nature Communications* 11: 5885.

Kupzig, S., V. Korolchuk, R. Rollason, A. Sugden, A. Wilde, and G. Banting. 2003. "Bst-2/HM1.24 Is a Raft-Associated Apical Membrane Protein With an Unusual Topology." *Traffic (Copenhagen, Denmark)* 4: 694–709.

Lo Cicero, A., C. Delevoye, F. Gilles-Marsens, et al. 2015. "Exosomes Released by Keratinocytes Modulate Melanocyte Pigmentation." *Nature Communications* 6: 7506.

Lopez, L. A., S. J. Yang, H. Hauser, et al. 2010. "Ebola Virus Glycoprotein Counteracts BST-2/Tetherin Restriction in a Sequence-Independent Manner That Does Not Require Tetherin Surface Removal." *Journal of Virology* 84: 7243–7255.

MacDonald, C., M. A. Stamnes, D. J. Katzmann, and R. C. Piper. 2015. "Tetraspan Cargo Adaptors Usher GPI-Anchored Proteins Into Multivesicular Bodies." *Cell Cycle* 14: 3673–3678.

Mahauad-Fernandez, W. D., K. A. DeMali, A. K. Olivier, and C. M. Okeoma. 2014. "Bone Marrow Stromal Antigen 2 Expressed in Cancer Cells Promotes Mammary Tumor Growth and Metastasis." *Breast Cancer Research* 16: 493.

Mahauad-Fernandez, W. D., and C. M. Okeoma. 2017. "Cysteine-Linked Dimerization of BST-2 Confers Anoikis Resistance to Breast Cancer Cells by Negating Proapoptotic Activities to Promote Tumor Cell Survival and Growth." *Cell Death & Disease* 8: e2687–e2687.

Mansouri, M., V. Kasinath, J. L. Douglas, et al. 2009. "Molecular Mechanism of BST2/Tetherin Downregulation by K5/MIR2 of Kaposi's Sarcoma-Associated Herpesvirus." *Journal of Virology* 83: 9672–9681.

Mathieu, M., N. Névo, M. Jouve, et al. 2021. "Specificities of Exosome Versus Small Ectosome Secretion Revealed by Live Intracellular Tracking of CD63 and CD9." *Nature Communications* 12: 4389.

McDonald, B., and J. Martin-Serrano. 2009. "No Strings Attached: The ESCRT Machinery in Viral Budding and Cytokinesis." *Journal of Cell Science* 122: 2167–2177.

Migliano, S. M., and D. Teis. 2018. "ESCRT and Membrane Protein Ubiquitination." *Progress in Molecular and Subcellular Biology* 57: 107–135.

Mitchell, R. S., C. Katsura, M. A. Skasko, et al. 2009. "Vpu Antagonizes BST-2-Mediated Restriction of HIV-1 Release via Beta-TrCP and Endo-Lysosomal Trafficking." *PLoS Pathogens* 5: e1000450.

Möbius, W., Y. Ohno-Iwashita, E. G. van Donselaar, et al. 2002. "Immunoelectron Microscopic Localization of Cholesterol Using Biotinylated and Non-Cytolytic Perfringolysin O." *Journal of Histochemistry and Cytochemistry* 50: 43–55.

Möbius, W., E. van Donselaar, Y. Ohno-Iwashita, et al. 2003. "Recycling Compartments and the Internal Vesicles of Multivesicular Bodies Harbor Most of the Cholesterol Found in the Endocytic Pathway." *Traffic (Copenhagen, Denmark)* 4: 222–231.

Morita, E., and W. I. Sundquist. 2004. "Retrovirus Budding." *Annual Review of Cell and Developmental Biology* 20: 395–425.

Muntasell, A., A. C. Berger, and P. A. Roche. 2007. "T Cell-Induced Secretion of MHC Class II-Peptide Complexes on B Cell Exosomes." *The EMBO Journal* 26: 4263–4272.

Neil, S. J. D., V. Sandrin, W. I. Sundquist, and P. D. Bieniasz. 2007. "An Interferon-α-Induced Tethering Mechanism Inhibits HIV-1 and Ebola Virus Particle Release but Is Counteracted by the HIV-1 Vpu Protein." *Cell Host & Microbe* 2: 193–203.

Neil, S. J. D., T. Zang, and P. D. Bieniasz. 2008. "Tetherin Inhibits Retrovirus Release and Is Antagonized by HIV-1 Vpu." *Nature* 451: 425–430.

Nolte-'t Hoen, E. N. M., S. I. Buschow, S. M. Anderton, W. Stoorvogel, and M. H. M. Wauben. 2009. "Activated T Cells Recruit Exosomes Secreted by Dendritic Cells via LFA-1." *Blood* 113: 1977–1981.

Olsén, E., B. García Rodríguez, F. Skärberg, et al. 2024. "Dual-Angle Interferometric Scattering Microscopy for Optical Multiparametric Particle Characterization." *Nano Letters* 24: 1874–1881.

Palmulli, R., H. K. Jackson, and J. R. Edgar. 2025. "Tethered Exosomes Containing the Matrix Metalloproteinase MT1-MMP Contribute to Extracellular Matrix Degradation." *Journal of Extracellular Vesicles* 14: e70122.

Pan, B. T., and R. M. Johnstone. 1983. "Fate of the Transferrin Receptor During Maturation of Sheep Reticulocytes In Vitro: Selective Externalization of the Receptor." *Cell* 33: 967–978.

Pardieu, C., R. Vigan, S. J. Wilson, et al. 2010. "The RING-CH Ligase K5 Antagonizes Restriction of KSHV and HIV-1 Particle Release by Mediating Ubiquitin-Dependent Endosomal Degradation of Tetherin." *PLoS Pathogens* 6: e1000843.

Peinado, H., M. Alečković, S. Lavotshkin, et al. 2012. "Melanoma Exosomes Educate Bone Marrow Progenitor Cells Toward a Pro-Metastatic Phenotype Through MET." *Nature Medicine* 18: 883–891.

Perez-Caballero, D., T. Zang, A. Ebrahimi, et al. 2009. "Tetherin Inhibits HIV-1 Release by Directly Tethering Virions to Cells." *Cell* 139: 499–511.

Perrin, P., L. Janssen, H. Janssen, et al. 2021. "Retrofusion of Intralumenal MVB Membranes Parallels Viral Infection and Coexists With Exosome Release." *Current Biology* 31: 3884–3893.e4.

Presle, A., S. Frémont, A. Salles, et al. 2021. "The Viral Restriction Factor Tetherin/BST2 Tethers Cytokinetic Midbody Remnants to the Cell Surface." *Current Biology* 31: 2203–2213.e5.

Prospéri, M.-T., C. Giordano, M. Gomez-Duro, et al. 2024. "Extracellular Vesicles Released by Keratinocytes Regulate Melanosome Maturation, Melanocyte Dendricity, and Pigment Transfer." *Proceedings of the National Academy of Sciences of the United States of America* 121: e2321323121.

Raiborg, C., and H. Stenmark. 2009. "The ESCRT Machinery in Endosomal Sorting of Ubiquitylated Membrane Proteins." *Nature* 458: 445–452.

Rajendran, L., M. Honsho, T. R. Zahn, et al. 2006. "Alzheimer's Disease Beta-Amyloid Peptides Are Released in Association With Exosomes." *Proceedings of the National Academy of Sciences of the United States of America* 103: 11172–11177.

Raposo, G., H. W. Nijman, W. Stoorvogel, et al. 1996. "B Lymphocytes Secrete Antigen-Presenting Vesicles." *Journal of Experimental Medicine* 183: 1161–1172.

Raposo, G., and W. Stoorvogel. 2013. "Extracellular Vesicles: Exosomes, Microvesicles, and Friends." *Journal of Cell Biology* 200: 373–383.

Salanueva, I. J., J. L. Carrascosa, and C. Risco. 1999. "Structural Maturation of the Transmissible Gastroenteritis Coronavirus." *Journal of Virology* 73: 7952–7964.

Seaman, M. N., J. M. McCaffery, and S. D. Emr. 1998. "A Membrane Coat Complex Essential for Endosome-to-Golgi Retrograde Transport in Yeast." *Journal of Cell Biology* 142: 665–681.

Stewart, H., R. Palmulli, K. H. Johansen, et al. 2023. "Tetherin Antagonism by SARS-CoV-2 ORF3a and Spike Protein Enhances Virus Release." *EMBO Reports* 24: e57224.

Stoorvogel, W., M. J. Kleijmeer, H. J. Geuze, and G. Raposo. 2002. "The Biogenesis and Functions of Exosomes." *Traffic (Copenhagen, Denmark)* 3: 321–330.

Stuffers, S., C. Sem Wegner, H. Stenmark, and A. Brech. 2009. "Multivesicular Endosome Biogenesis in the Absence of ESCRTs." *Traffic (Copenhagen, Denmark)* 10: 925–937.

Theos, A. C., S. T. Truschel, D. Tenza, et al. 2006. "A Lumenal Domain-Dependent Pathway for Sorting to Intralumenal Vesicles of Multivesicular Endosomes Involved in Organelle Morphogenesis." *Developmental Cell* 10: 343–354.

Théry, C., S. Amigorena, G. Raposo, and A. Clayton. 2006. "Isolation and Characterization of Exosomes From Cell Culture Supernatants and Biological Fluids." *Current Protocols in Cell Biology*, Chapter 3: Unit 3.22.

Théry, C., L. Duban, E. Segura, P. Véron, O. Lantz, and S. Amigorena. 2002. "Indirect Activation of Naïve CD4+ T Cells by Dendritic Cell-Derived Exosomes." *Nature Immunology* 3: 1156–1162.

van Niel, G., S. Charrin, S. Simoes, et al. 2011. "The Tetraspanin CD63 Regulates ESCRT-Independent and -Dependent Endosomal Sorting During Melanogenesis." *Developmental Cell* 21: 708–721.

van Niel, G., S. Charrin, S. Simoes, et al. 2011. "The Tetraspanin CD63 Regulates ESCRT-Independent and -Dependent Endosomal Sorting During Melanogenesis." *Developmental Cell* 21: 708–721.

Verweij, F. J., M. P. Bebelman, C. R. Jimenez, et al. 2018. "Quantifying Exosome Secretion From Single Cells Reveals a Modulatory Role for GPCR Signaling." *Journal of Cell Biology* 217: 1129–1142.

Wang, S. M., K. J. Huang, and C. T. Wang. 2014. "BST2/CD317 Counteracts Human Coronavirus 229E Productive Infection by Tethering Virions at the Cell Surface." *Virology* 449: 287–296.

Welbourn, S., S. Kao, K. E. Du Pont, A. J. Andrew, C. E. Berndsen, and K. Strebel. 2015. "Positioning of Cysteine Residues Within the N-Terminal Portion of the BST-2/Tetherin Ectodomain Is Important for Functional Dimerization of BST-2*." *Journal of Biological Chemistry* 290: 3740–3751.

Welsch, S., O. T. Keppler, A. Habermann, I. Allespach, J. Krijnse-Locker, and H.-G. Kräusslich. 2007. "HIV-1 Buds Predominantly at the Plasma Membrane of Primary Human Macrophages." *PLoS Pathogens* 3, no. 3: e36.

Supporting Information

Additional supporting information can be found online in the Supporting Information section.

Supporting Information File 1: boc70046-sup-0001-SuppMat.pdf